REPORT DOCUMENTATION PAGE

Form Approved
OMB No. 0704-0188

1. AGENCY USE ONLY (Leave blank)	2. REPORT DATE	3. REPORT TYPE AND DATES COVERED
	2/27/96	Final Tech. Rpt. 5/15/92-8/15/95

4. TITLE AND SUBTITLE

(U) Atomization of Viscous Liquid Sheets

5. FUNDING NUMBERS

PE - 61102F
PR - 2308
SA - BS
G - F49620-92-J-0194

6. AUTHOR(S)

Essam A. Ibrahim

7. PERFORMING ORGANIZATION NAME(S) AND ADDRESS(ES)

Tuskegee University
Tuskegee, AL 36088

8. PERFORMING ORGANIZATION

AFOSR-TR-96
0278

9. SPONSORING/MONITORING AGENCY NAME(S) AND ADDRESS(ES)

AFOSR/NA
110 Duncan Avenue, Suite B115
Bolling AFB, DC 20332-0001

10. SPONSORING/MONITORING AGENCY REPORT NUMBER

92-J-0194

11. SUPPLEMENTARY NOTES

12a. DISTRIBUTION/AVAILABILITY STATEMENT

Approved for public release; distribution is unlimited

12b. DISTRIBUTION CODE

13. ABSTRACT (Maximum 200 words)

The atomization of liquid sheets is investigated via the linear and nonlinear instability theory. It is found that liquid viscosity reduces the growth rate and dominant wave number of disturbances. An increase in the gas-to-liquid density ratio raises the growth rate of disturbances. Surface tension always opposes the development of instability. Sinuous waves dominate the instability process at large We number. The results of the nonlinear theory indicate that maximum thinning and subsequent rupture of the sheet into ligaments occur at positions corresponding to half the length of the fundamental waves. The growth of disturbances corresponds to a combination of a basic sinuous mode and a dilational first harmonic. The mechanisms of disintegration of constant thickness and attenuating liquid sheets are studied. The sheet breakup length, the size of the drops, and the spray angle produced by its disintegration are estimated. Both the breakup length and the drop size decrease as We number is increased. The spray angle is reduced by increasing We number. The present theoretical predictions are compared with empirical correlations and experimental data and good agreement is observed.

14. SUBJECT TERMS

Atomization, Liquid Sheet, Drop Size, Breakup Length, Spray Angle, Spray Characteristics

15. NUMBER OF PAGES

51

16. PRICE CODE

17. SECURITY CLASSIFICATION OF REPORT	18. SECURITY CLASSIFICATION OF THIS PAGE	19. SECURITY CLASSIFICATION OF ABSTRACT	20. LIMITATION OF ABSTRACT
Unclassified	Unclassified	Unclassified	UL

NSN 7540-01-280-5500

Standard Form 298 (890104 Draft)
Prescribed by ANSI Std. 239-18
298-01

STATEMENT OF WORK

* Study the fundamental mechanisms of atomization of viscous liquid sheets such as those produced by gas-burner nozzles. The proposed approach employs the theory of nonlinear spatial instability cast in a simplified formulation through the utilization of physically sound assumptions.

* Obtain a proven numerical solution of the governing equations coded in computer language. The code would accept input such as sheet properties, thickness and initial velocity. As output, the code would compute the size and velocity of the drops produced by the liquid sheet breakup.

* Validate the computed values of drop size and velocity by comparison with experimental data.

* Investigate the phenomenon of bi-modal atomization in which two prevalent drop sizes are observed as a result of sheet disintegration.

* Conduct a parametric study to examine the influence of liquid fuel properties such as density, viscosity and surface tension on the outcome of sheet atomization.

INTRODUCTION

Atomization is a process whereby a volume of liquid is converted into a multiplicity of small drops. One of the most important applications of atomization is liquid fuel injection in internal combustion engines, gas turbines, and liquid-propellant rocket engines. In this case, the principal aim of the atomization process is to produce a high ratio of surface-to-mass in the liquid phase, which results in very high evaporation rates that contribute to raising the combustion efficiency and reducing environmental pollution.

In internal combustion engines, the liquid fuel is injected from an orifice in the form of a circular jet. The mechanism of breakup of circular liquid jets has been extensively studied.[1-5] Gas burners used in gas-turbine combustors employ swirl nozzles that cause the liquid fuel to be issued as a thin hollow-cone sheet. Most of the important features of sheet breakup processes in hollow-cone sprays may be reasonably understood by studying the stability of a moving thin liquid sheet of constant thickness.[6-7]

Despite its practical significance, there has been little theoretical investigation of the breakup of a liquid sheet. The basic study by Squire[6] treats the instability of an inviscid liquid sheet. Hagerty and Shea[8] conducted an experimental and theoretical study on a flat sheet of liquid produced by a slender orifice that was subjected to waves of different frequency. They concluded that only two types of waves are possible at any given frequency. Either the two surfaces of the sheet are in phase to produce antisymmetrical (sinusoidal) waves, or they oscillate out of phase to produce symmetrical (dilational) waves. Their results show that the principal sources of sheet instability are the aerodynamic forces arising from the interaction of the sheet with the sheet with surrounding as medium. Taylor[7] analyzed the growth of wind-induced interface waves under the assumption of potential flow in the liquid and the surrounding gas with a discontinuity in velocity at the interface. Dombrowski and Johns[9] extended the analysis by including the effect of liquid viscosity and sheet thickness attenuation. However, Dombrowski and Johns[9] results are only valid for large gas Weber number (ratio of the aerodynamic forces in the gas to the capillary forces in the liquid) owing to approximations made in their analysis.[10] Clark and Dombrowski[11] have applied a second-order perturbation theory to the calculate the breakup lengths of attenuating sheets for the case where the wavelengths are relatively long compared with the sheet thickness. The large-amplitude theory of Crapper et al.[12] is restricted to a steady-state situation that the instability waves never really reach. Rangel and Sirignano[13, 14] studied the effect of surface tension and density ratio on the nonlinear temporal growth of Kelvin-Helmholtz instability waves using the vortex-sheet discretization technique. Rangel and Hess[15] used the same technique to investigate the

nonlinear spatial instability of a liquid sheet. However, this technique is only applicable to inviscid flow. Li and Tankin[10] presented a study of the temporal instability of a viscous liquid sheet of constant thickness that is valid at any Weber number. Li and Tankin[10] concluded that antisymmetrical perturbations control the instability process for large Weber numbers, whereas the symmetrical perturbations dominate for small Weber numbers. The absolute and convective instability of a viscous liquid sheet has been investigated by Lin et al.[16]

Crapper et al.[17] advanced experimental evidence that the growth of instability waves on liquid sheets takes place spatially, not temporally. It is now well recognized tat both temporal and spatial growth need consideration in general.[18-20] The author is only aware of one attempt to investigate the spatial instability of a viscous liquid sheet, namely that of Chuech.[21]. Chuech revised the temporal analysis of Dombrowski and Johns[9] to study the spatial instability of a viscous liquid sheet. However, Chuech's analysis is based on the same assumptions introduced by Dombrowski and Johns that lends his results also to be valid only for large Weber numbers. The present work is motivated by the need to develop a fundamental understanding of the spatial instability of liquid sheets that is at least at the same level of our understanding of temporal instability. The basic features of the spatial instability as well as the differences and similarities between spatial and temporal instability of a liquid sheet are investigated.

LINEAR ANALYSIS

Consider a viscous liquid sheet of thickness 2a that is issued from a nozzle at a relative velocity U into a quiescent inviscid gas medium as shown in Figs. 1 and 2. The gas viscosity is neglected following Taylor's[2] treatment of a related problem. This neglect of gas viscosity is based on the observation that the gas viscosity is weakly stabilizing, as has been demonstrated by Tomotika[22] and Lin and Ibrahim.[5] U is small compared to the velocity of sound, thus the assumption of incompressibility for both fluids is valid. Assume u, v are the liquid velocity components in the x, y directions, respectively, resulting from a disturbance, and p the pressure due to the disturbance. The x axis is parallel to the direction of U, and the y axis is normal to the undisturbed sheet surface with its origin at the midplane of the sheet. The equations of mass and momentum conservation that govern the liquid motion are linearized by neglecting all nonlinear terms in disturbance quantities, and may be written, respectively, as

$$\frac{\partial u}{\partial x} + \frac{\partial v}{\partial y} = 0 \qquad (1)$$

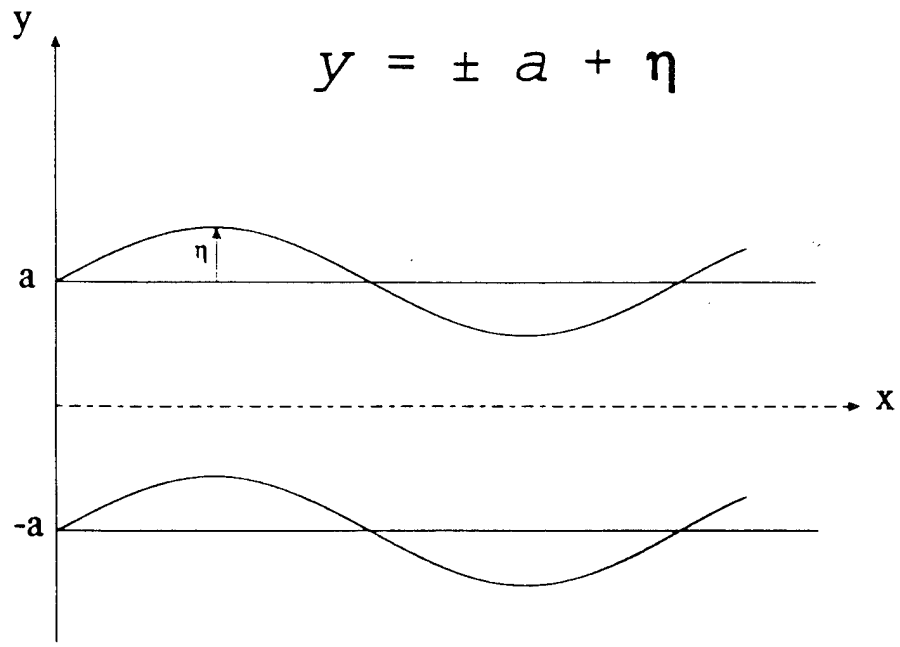

Figure 1. Antisymmetrical disturbances.

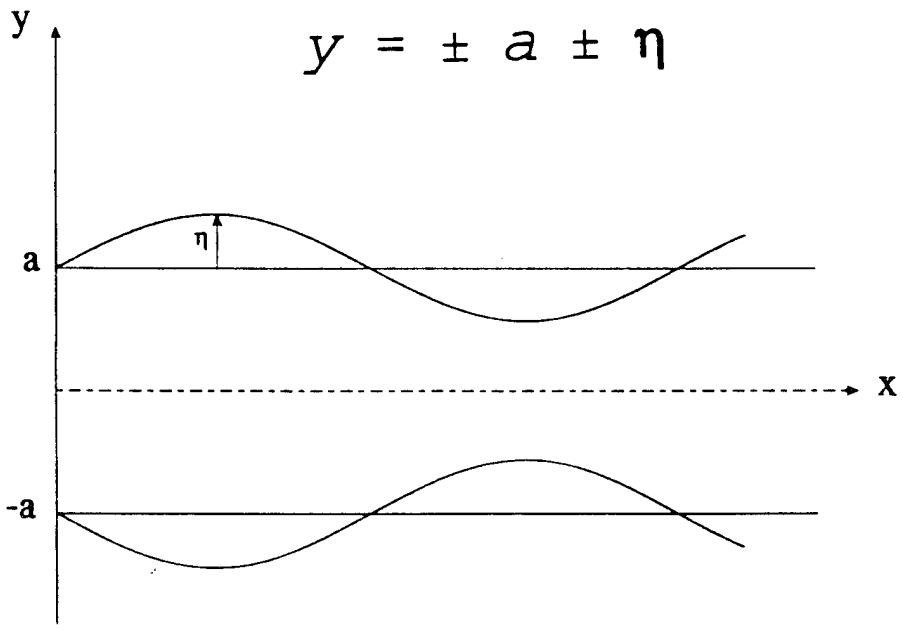

Figure 2. Symmetrical disturbances.

$$\frac{\partial u}{\partial t} + U\frac{\partial u}{\partial x} = -\frac{1}{\rho_\ell}\frac{\partial p}{\partial x} + \nu_\ell\left(\frac{\partial^2 u}{\partial x^2} + \frac{\partial^2 u}{\partial y^2}\right) \quad (2)$$

$$\frac{\partial v}{\partial t} + U\frac{\partial v}{\partial x} = -\frac{1}{\rho_\ell}\frac{\partial p}{\partial y} + \nu_\ell\left(\frac{\partial^2 v}{\partial x^2} + \frac{\partial^2 v}{\partial y^2}\right) \quad (3)$$

where t is the time, and ρ_ℓ, ν_ℓ are the liquid density and kinematic viscosity, respectively. The boundary conditions that Eqs. (1-3) are subjected to depend on whether the sheet disturbance is antisymmetrical or symmetrical as can be seen from Figs. 1 and 2. For antisymmetrical disturbances, the displacements of corresponding points on the two interfaces are equal in magnitude and in the same direction. For symmetrical disturbances the displacements are equal but occur in opposite directions. Therefore, for antisymmetrical disturbances the two interfaces are regarded to have the following form:

$$y = a + \eta, \quad y = -a + \eta \quad (4)$$

For Symmetrical disturbances the two interfaces have the form

$$y = a + \eta, \quad y = -a - \eta \quad (5)$$

where η is he interface displacement at time t and distance x along the interface. The boundary conditions for Eqs.(1-3) at the two interfaces, which may be taken as $y \approx \pm a$, are that the velocity v at the interface is equal to the total derivative of the interface displacement. Since the surrounding gas medium is assumed to be inviscid, the tangential stresses should vanish at the interfaces. The normal stresses across the interface should be balanced. For antisymmetrical disturbances, these boundary conditions may be written, respectively, as

$$v = \frac{\partial \eta}{\partial t} + U\frac{\partial \eta}{\partial x} \quad at \quad y \approx \pm a \quad (6)$$

$$\mu_\ell\left(\frac{\partial u}{\partial y} + \frac{\partial v}{\partial x}\right) = 0 \quad at \quad y \approx \pm a \quad (7)$$

$$-p + 2\mu_\ell\frac{\partial v}{\partial y} = -p_g + p_\sigma \quad at \quad y \approx \pm a \quad (8)$$

where μ_ℓ is the liquid dynamic viscosity, p_g is the gas pressure, and p_σ is the pressure due to surface tension. For symmetrical disturbances, the only boundary condition that changes form is the

kinematic condition at y ≈ -a, which becomes

$$v = -\left(\frac{\partial \eta}{\partial t} + U\frac{\partial \eta}{\partial x}\right) \quad at \quad y \approx -a \tag{9}$$

in accordance with the form of Eq. (5). The stream function of the liquid motion ψ is given by

$$u = \frac{\partial \psi}{\partial y} \quad , \quad v = -\frac{\partial \psi}{\partial x} \tag{10}$$

The equation of mass conservation Eq. (1) is readily satisfied by substitution from Eq. (10). The stream function may be represented by its Fourier series components and we may focus our attention on one of these components, which is written as

$$\psi = \Psi(y)\exp(ikx + \omega t) \tag{11}$$

For spatial instability analysis, k is a complex variable $k = k_r + ik_i$, and is an imaginary variable $\omega = i\omega_i$. The real part of k, k_r represents the wave number (2π divided by the wavelength) of the disturbance, and the imaginary part k_i represents the rate of growth or decay of the disturbance depending on whether k_i is negative or positive, respectively. The imaginary variable ω_i is 2π times the disturbance frequency, $-\omega_i/k_r$ is the wave propagation velocity, and $-\partial\omega_i/\partial k_r$ is the group velocity of the disturbances. Similarly, the interfacial displacement may be expressed as

$$\eta = \eta_0 \exp(ikx + \omega t) \tag{12}$$

where η_0 is the amplitude of the initial disturbance. Eliminating the pressure from Eqs.(2) and (3) by cross differentiation and then substituting from Eq. (11) we get

$$\frac{\partial^4 \Psi(y)}{dy^4} - (s^2 + k^2)\frac{\partial^2 \Psi(y)}{dy^2} + k^2 s^2 \Psi(y) = 0 \tag{13}$$

$$s^2 = \left(k^2 + \frac{\omega}{\nu_\ell} + \frac{ikU}{\nu_\ell}\right) \tag{14}$$

The general solution of Eq. (13) is given by

$$\Psi(y) = \left[\left(C_1 e^{ky} + C_2 e^{-ky}\right) + \left(C_3 e^{sy} + C_4 e^{-sy}\right)\right] \tag{15}$$

where C_1, C_2, C_3, and C_4 are constants of integration that are determined from the boundary conditions (6) and (7) in accordance with Eqs. (10-12), (14), and (15) to be

$$C_1 = C_2 = i\eta_0 \nu_\ell \frac{(k^2 + s^2)}{2k \cosh(ka)} \tag{16}$$

$$C_3 = C_4 = -i\eta_0 \nu_\ell \frac{k}{\cosh(sa)} \tag{17}$$

Substituting from Eqs.(15-17) into Eq.(11) we get the stream function of liquid motion as

$$\psi = 2[C_1 \cosh(ky) + C_2 \cosh(sy)] \exp(ikx + \omega t) \tag{18}$$

where C_1 and C_2 are given by Eqs. (16) and (17), respectively. The liquid pressure due to disturbance, p, may be represented by

$$p = P(y) \exp(ikx + \omega t) \tag{19}$$

in accordance with the form of Eq. (11). The pressure p may now be determined from either Eq. (2) or (3) by substitution from Eqs. (10), (11), (16-19) to yield

$$p = 2i\rho_\ell(\omega + ikU) C_1 \sinh(ky) \exp(ikx + \omega t) \tag{20}$$

In the present analysis, the effect of the surrounding gas medium on the instability of liquid sheet is through the normal stress in boundary conditio (8). The gas medium is assumed to be inviscid and quiescent before the disturbances set in. The mass conservation equation is then

$$\frac{\partial u_g}{\partial x} + \frac{\partial v_g}{\partial y} = 0 \tag{21}$$

where subscript g denotes quantities for the gas medium.

The gas velocity can be expressed in terms of a velocity potential, ϕ_g, such that

$$u_g = \frac{\partial \phi_g}{\partial x}, \qquad v_g = \frac{\partial \phi_g}{\partial y} \tag{22}$$

Furthermore, the velocity potential for the inviscid gas motion is assumed to be

$$\phi_g = \Phi_g(y) \exp(ikx + \omega t) \tag{23}$$

The boundary conditions for the inviscid gas require that across the liquid-gas interface the y-component velocity be continuous, and far away from the liquid surface the disturbances decay to zero. Hence, the boundary conditions for the upper-half plane are

$$v_g = \frac{\partial \phi_g}{\partial y} = \frac{\partial \eta}{\partial t} \quad at \quad y \approx a \tag{24}$$

$$v_g = \frac{\partial \phi_g}{\partial y} = 0 \quad at \quad y \to \infty \tag{25}$$

Substituting from Eq. (22) into Eq. (21) and the boundary conditions (24) and (25) yields

$$\phi_g = -\frac{\omega}{k} \exp[(k(a - y)]\eta_0 \exp(ikx + \omega t) \tag{26}$$

The gas pressure may be calculated from the integrated momentum equation for the gas medium

$$p_g = -\rho_g \frac{\partial \phi_g}{\partial t} \tag{27}$$

which upon substitution from Eq. (26) gives

$$p_g = ro_g \frac{\omega^2}{k} \exp[k(a - y)]\eta_0 \exp(ikx + \omega t) \tag{28}$$

The pressure induced by surface tension is, to the first order in η

$$p_\sigma = \frac{\sigma}{R} \approx \sigma \frac{\partial^2 \eta}{\partial \eta^2} = -\sigma k^2 \eta_0 \exp(ikx + \omega t) \quad at \quad y \approx a \tag{29}$$

where σ is the surface tension, and R is the radius of curvature of the liquid-gas interfaces. Substitution from Eqs. (10), (16-18), (20), (28), and (29) into the normal stress boundary condition (8) for y = a, leads to the following dispersion relation between k and ω:

$$\begin{aligned}&[\rho_\ell(\omega + ikU) + 2\mu_\ell k^2][\nu_\ell(k^2 + s^2)] \tanh(ka) \\ &\quad - 4\mu_\ell \nu_\ell k^3 s \tanh(sa) + \rho_g \omega^2 + \sigma k^3 = 0\end{aligned} \tag{30}$$

The derivation process of the dispersion relation for the symmetrical disturbances is very similar to that of antisymmetrical ones. The governing equations are exactly the same, but the kinematic boundary condition for the liquid phase at y = -a is different, as pointed out earlier in connection with Eq. (9). The dispersion relation for symmetrical disturbances is similar to Eq. (30) except that tanh(ka) and tanh(sa) are replaced by coth(ka) and coth(sa), respectively:

$$\left[\rho_\ell(\omega + ikU) + 2\mu_\ell k^2\right]\left[\nu_\ell(k^2+s^2)\right]\coth(ka) - 4\mu_\ell\nu_\ell k^3 s\coth(sa) + \rho_g\omega^2 + \sigma k^3 = 0 \quad (31)$$

Equations (3) and (31) are similar to Eqs. (37) and (38) of Li and Tankin,[10] except that is purely imaginary and k is complex for the present spatial analysis, while is complex and k is real in Li and Tankin's[10] temporal analysis. However, the derivation procedure of Eqs. (30) and (31) in the present investigation is quite different from that of Li and Tankin. In their formulation, Li and Tankin determined the pressure in the viscous liquid from the relations applicable to inviscid liquid because the presence of viscosity affects the wave frequency, but not the pressure within the liquid as pointed out by Levich.[23] Although their approach is correct, it is unnecessary and it leads to a more complicated derivation. The present formulation allows for direct evaluation of the viscous liquid pressure via the stream function of the liquid motion.

RESULTS AND DISCUSSION

To facilitate the analysis, Eqs. (3) and (31) are respectively expressed in dimensionless form as follows:

$$\frac{m_1^2}{Re^2}\tanh(K) - \frac{4m_1^{1/2}}{Re^2}K^3\tanh(m^{1/2}) - \rho\Omega_i^2 + \frac{\rho}{We_g}K^3 = 0 \quad (32)$$

$$\frac{m_1^2}{Re^2}\coth(K) - \frac{4m^{1/2}}{Re^2}K^3\coth(m^{1/2}) - \rho\Omega_i^2 - \frac{\rho}{We_g}K^3 = 0 \quad (33)$$

where $\Omega_i = \omega_i(a/U)$, $K = K_r + iK_i = (k_r + ik_i)a = ka$, $\rho = (\rho_g/\rho_\ell)$, $m = [K^2 + iRe(\Omega_i + K)]$, $m_1 = m + K^2$. Re is the liquid Reynolds number $Re = Ua/\nu_\ell$, and We_g is the gas Weber number $We_g = \rho_g U^2 a/\sigma$. For an inviscid liquid sheet, $Re\to\infty$ and Eqs. (32) and (33) reduce to

$$-(\Omega_i + K)^2\tanh(K) - \rho\Omega_i^2 + \frac{\rho}{We_g}K^3 = 0 \quad (34)$$

$$-(\Omega_i + K)^2\coth(K) - \rho\Omega_i^2 + \frac{\rho}{We_g}K^3 = 0 \quad (35)$$

respectively. Equations (32-35) are solved numerically using Muller's[24] method to yield values of K as a function of Ω_i for different values of the dimensionless parameters ρ, Re, and We_g. The IMSL Fortran subroutine ZANLY uses Muller's[24] method with deflation to find a real or complex root of an arbitrary complex function

given an initial guess of the root (i. e., $K = K_r + iK_i$). In providing the guessed root it is helpful to realize that $k_r \approx -\omega_i$ in accordance with Gaster's[25] theorem.

Figure 3 shows a comparison between the predictions of the spatial and temporal growth rates of antisymmetrical disturbances for ρ = 0.1, We_g = 4.0, and Re = ∞, 63.25. A similar comparison for symmetrical disturbances is shown in Fig. 4. Equations (39-42) of Li and Tankin[10] are used to obtain the temporal growth rate results shown in Figs. 3 and 4. However, the temporal growth rate of Li and Tankin was divided by the square root of the liquid Weber number $We\ell = \rho_\ell U^2 a/\sigma = We_g/\rho$, to be made dimensionless in the same manner as the present spatial growth rate.

It can be seen from Figs. 3 and 4 that, for an inviscid liquid sheet, the spatial instability growth rate and limiting wave number are always larger than that of temporal instability. The effect of viscosity in the liquid is to cause the growth rates of both spatial and temporal instability are identical and equal to We_g for viscous liquid sheets. Note that the limiting wave number can be obtained by setting $K_i = 0$ in Eq. (32) or (33) for antisymmetrical disturbances, respectively. Both Eq. (32) or (33) give the limiting wave number as $K_r = We_g$.

Li and Tankin[10] have shown that the limiting wave number of temporal instability is also equal to We_g for both antisymmetrical and symmetrical disturbances. For inviscid liquid sheets undergoing spatial instability the limiting wave number is a function of ρ, We_g, and Ω_i, as can be seen from Eqs. (34) and (35). It is not possible to eliminate Ω_i from Eqs. (34) or (35) by separation of each of the equations into real and imaginary components as has been done in the temporal instability analysis of Li and Tankin.

The effects of liquid viscosity on the spatial instability of liquid sheets is investigated further in Figs. 5 and 6 for antisymmetrical and symmetrical disturbances, respectively, for ρ = 0.1, We_g = 4.0, and Re = ∞, 63.25, 1.25. It is seen from Figs. 5 and 6 that liquid viscosity, affected through Reynolds number, reduces the disturbance growth rate and shifts the dominant wave number of the disturbances to a longer wavelength. The limiting wave number of inviscid liquid sheets is less than that of viscous liquid sheets, which is fixed at $K_r = We_g$ as discussed earlier. In their photographical study of the disintegration of liquid sheets, Dombrowski and Fraser[26] concluded that increasing liquid viscosity yields a more stable sheet in agreement with the present results. This damping effect of viscosity is due to its role as a mechanism of energy dissipation.

Squire[9] reported that when the gas Weber number falls below a critical value $We_g = \rho$, there will be no instability arising from the antisymmetrical long-wave disturbances of an inviscid liquid

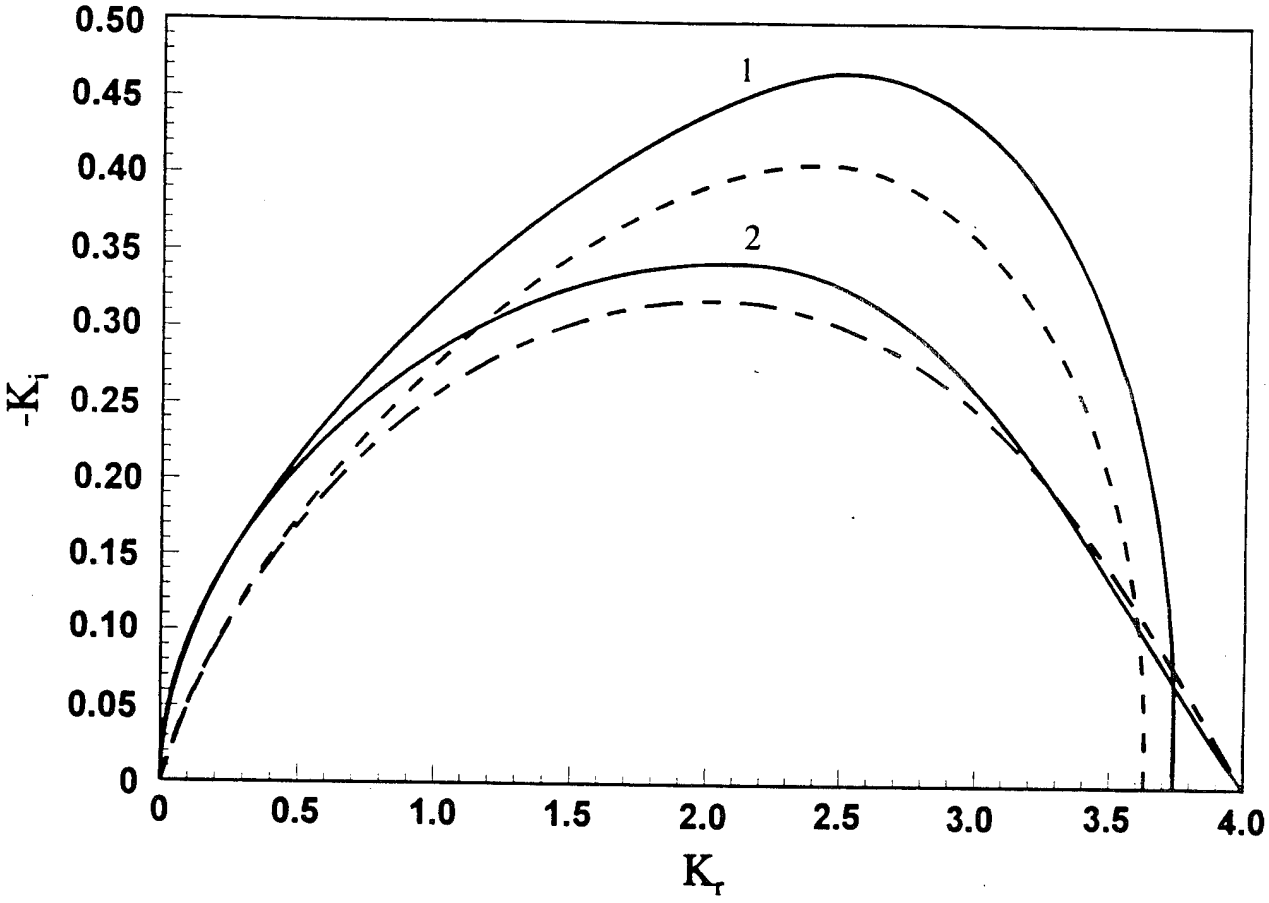

Figure 3. Comparison of spatial and temporal instability of antisymmetrical disturbances. ρ = 0.1 and We_g = 4.0. Curve 1, spatial, Re = ∞, curve 2, spatial, Re = 63.25, dashed curve, temporal, Re = ∞, centerlined curve, temporal, Re = 63.25.

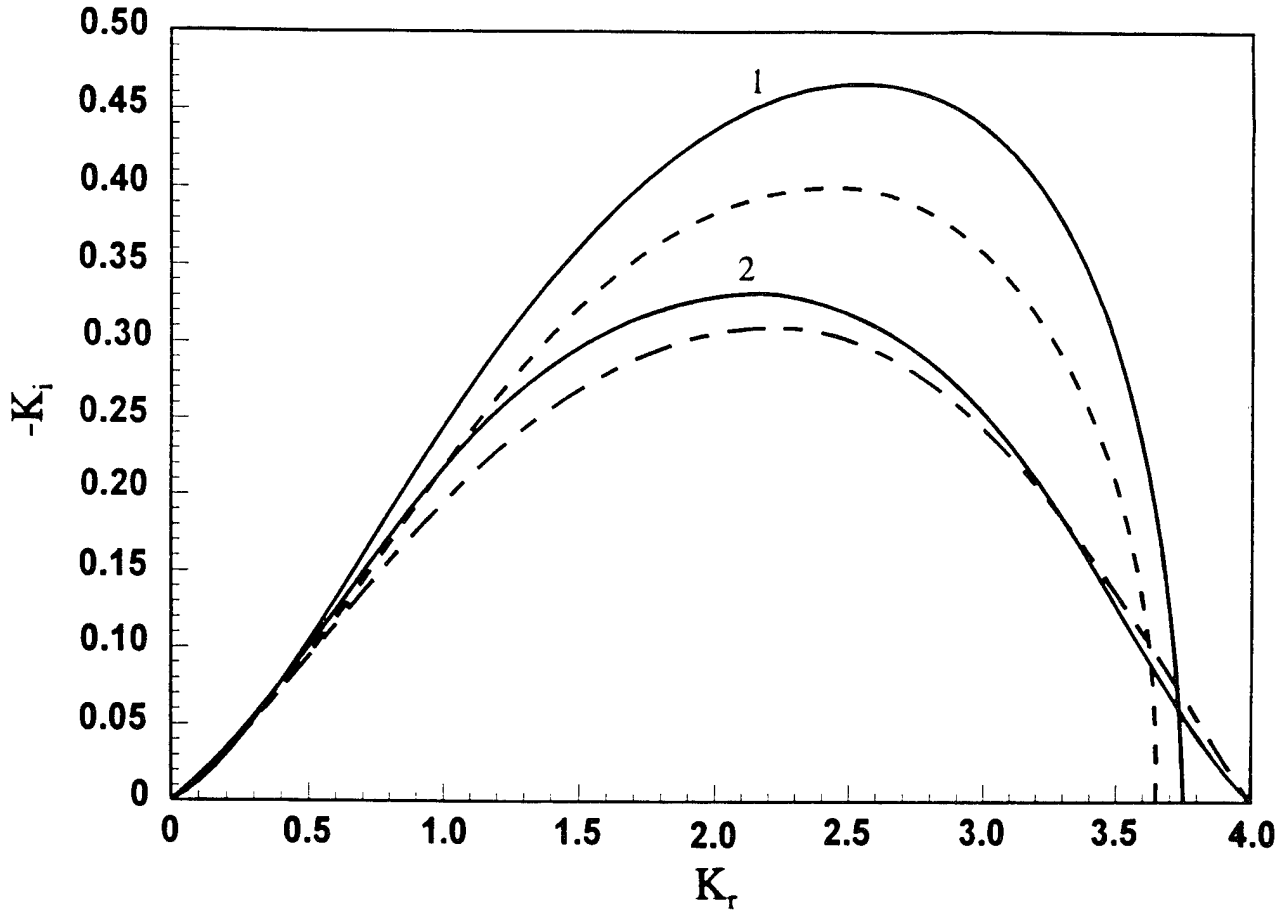

Figure 4. Comparison of spatial and temporal instability of symmetrical disturbances. $\rho = 0.1$ and $We_g = 4.0$. Curve 1, spatial, Re = ∞, curve 2, spatial, Re = 63.25, dashed curve, temporal, Re = ∞, centerlined curve, temporal, Re = 63.25.

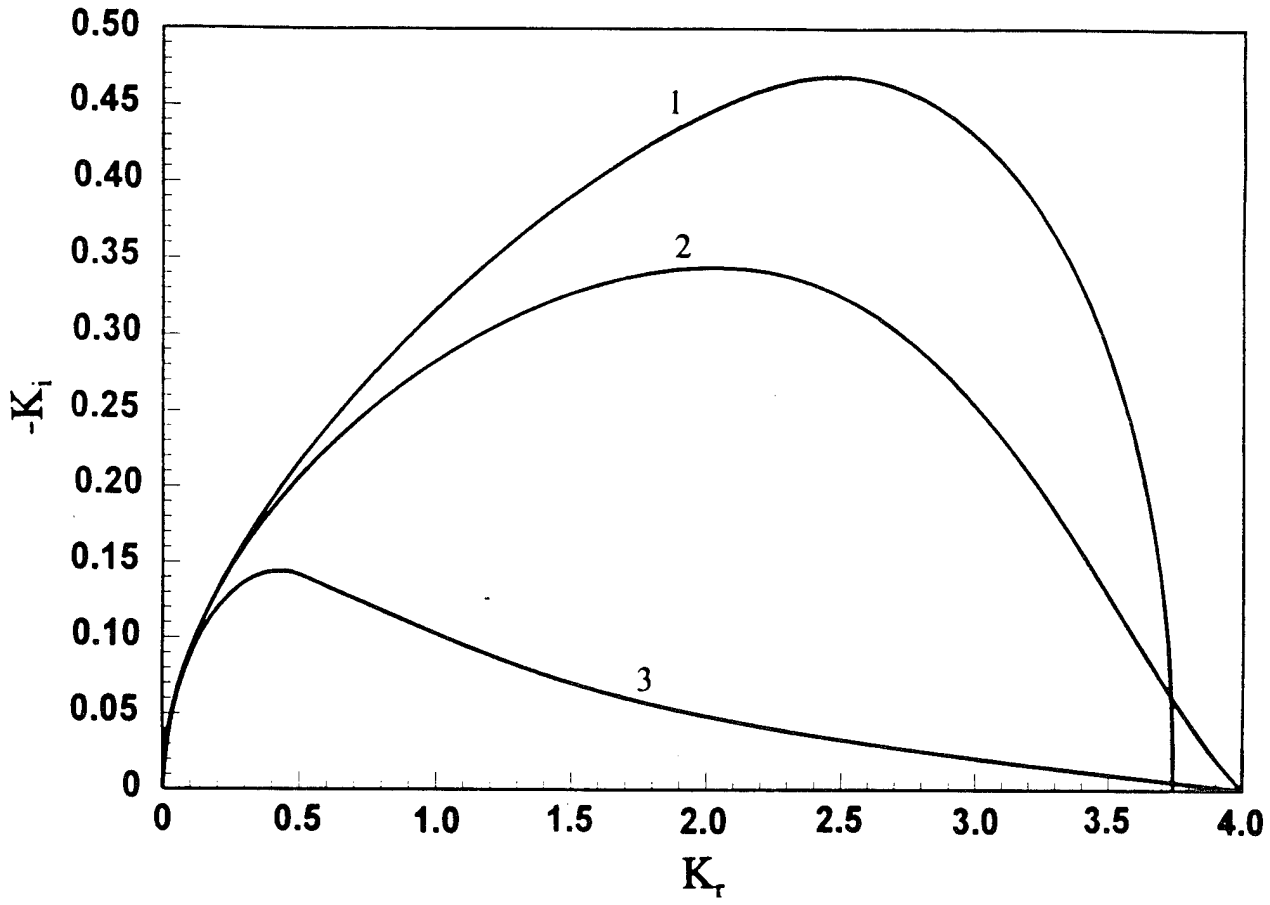

Figure 5. Effect of liquid viscosity on antisymmetrical disturbances. $\rho = 0.1$ and $We_g = 4.0$. Curve 1, Re = ∞, curve 2, Re = 63.25, curve 3, Re = 1.25.

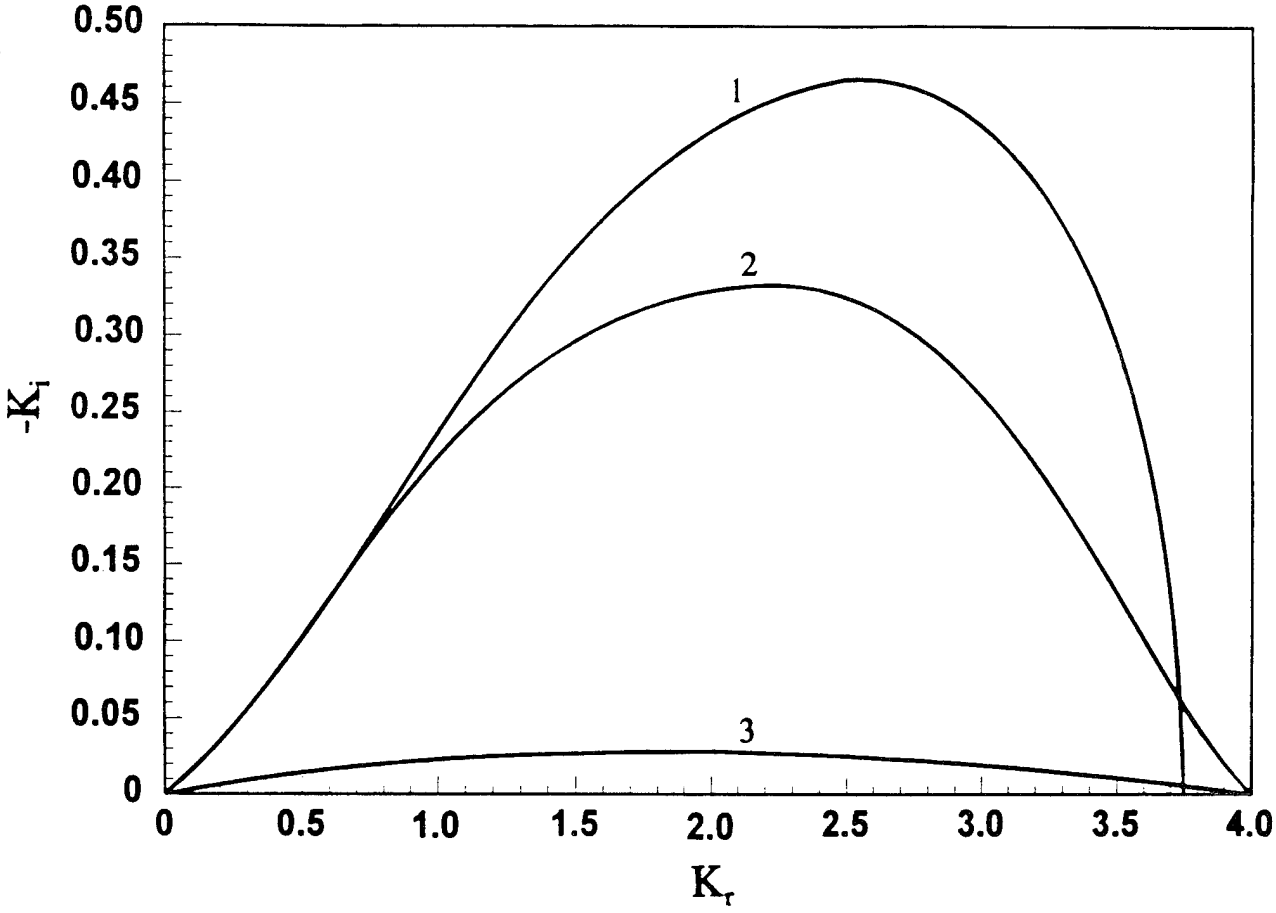

Figure 6. Effect of liquid viscosity on symmetrical disturbances. $\rho = 0.1$ and $We_g = 4.0$. Curve 1, Re = ∞, curve 2, Re = 63.25, curve 3, Re = 1.25.

sheet. For a viscous liquid sheet subjected to antisymmetrical disturbances, Li and Tankin[10] observed that if the gas Weber number is slightly larger than its critical value, there exists two local maxima for the growth rate of the disturbance. These two different modes of instability were termed aerodynamic and viscosity-enhanced by Li and Tankin. At low gas Weber number, $We_g \approx \rho$, liquid viscosity has little effect on the aerodynamic mode of instability, and growth rates of inviscid and viscous liquid sheets are essentially the same. At high gas Weber number, the aerodynamic instability is hindered by liquid viscosity as has been discussed with regard to Figs. 4 and 5. The viscosity-enhanced mode is characterized by the increase of the growth rate of the disturbances with viscosity. At gas Weber numbers less than the critical value $We_g = \rho$, aerodynamic instability disappears completely, and only viscosity-enhanced instability will exist.

To explore the existence of the such double modes in the spatial instability arising from antisymmetrical disturbances, computations have been carried out for $\rho = 0.1$, $We_g = 0.13$, and Re = 0.2, 0.25, using Eq. (32). The results are depicted in Figs. 7 and 8, which show the aerodynamic and viscosity-enhanced instabilities, respectively. Although these two modes of instabilities occur simultaneously, they are plotted separately in Figs. 7 and 8 because the magnitude of the growth rate of aerodynamic instability are much larger than that of viscosity-enhanced. However, Li and Tankin[10] demonstrated that the viscosity-enhanced mode dominated the instability process when the gas Weber number is slightly above the critical value $We_g = \rho$, specifically at $We_g = 0.1025$ and $\rho = 0.1$. As Weber number is increased aerodynamic instability continues to grow while the viscosity-enhanced instability is greatly diminished.

For symmetrical disturbances, the growth rate curves are always similar to those shown in Fig. 6, whether the gas Weber number is small or large. Aerodynamic instability always prevails, and viscosity-enhanced instability has no local maximum growth rate. There is no critical value of Weber number for symmetrical disturbances.

Figure 9 and 10 illustrate the effect of gas-to-liquid density ratio on the growth rates of spatial instability due to antisymmetrical and symmetrical disturbances, respectively. The data in Figs. 9 and 10 correspond to $We_g = 0.9$ and Re = 1.0. The density ratio varies as $\rho = 2.0, 1.0, 0.1, 0.01$ for antisymmetrical disturbances, and $\rho = 1.0, 0.1$, and 0.05 for symmetrical disturbances. It is seen in Fig. 9 that an increase in the gas-to-liquid density ratio increases the growth rate and dominant wave number of the antisymmetrical disturbances as long as the density ratio is less than the gas Weber number. Once the density ratio becomes greater than the gas Weber number the disturbance growth rate is reduced with further increase of the density ratio. A density ratio higher than the gas Weber number shifts the mechanism

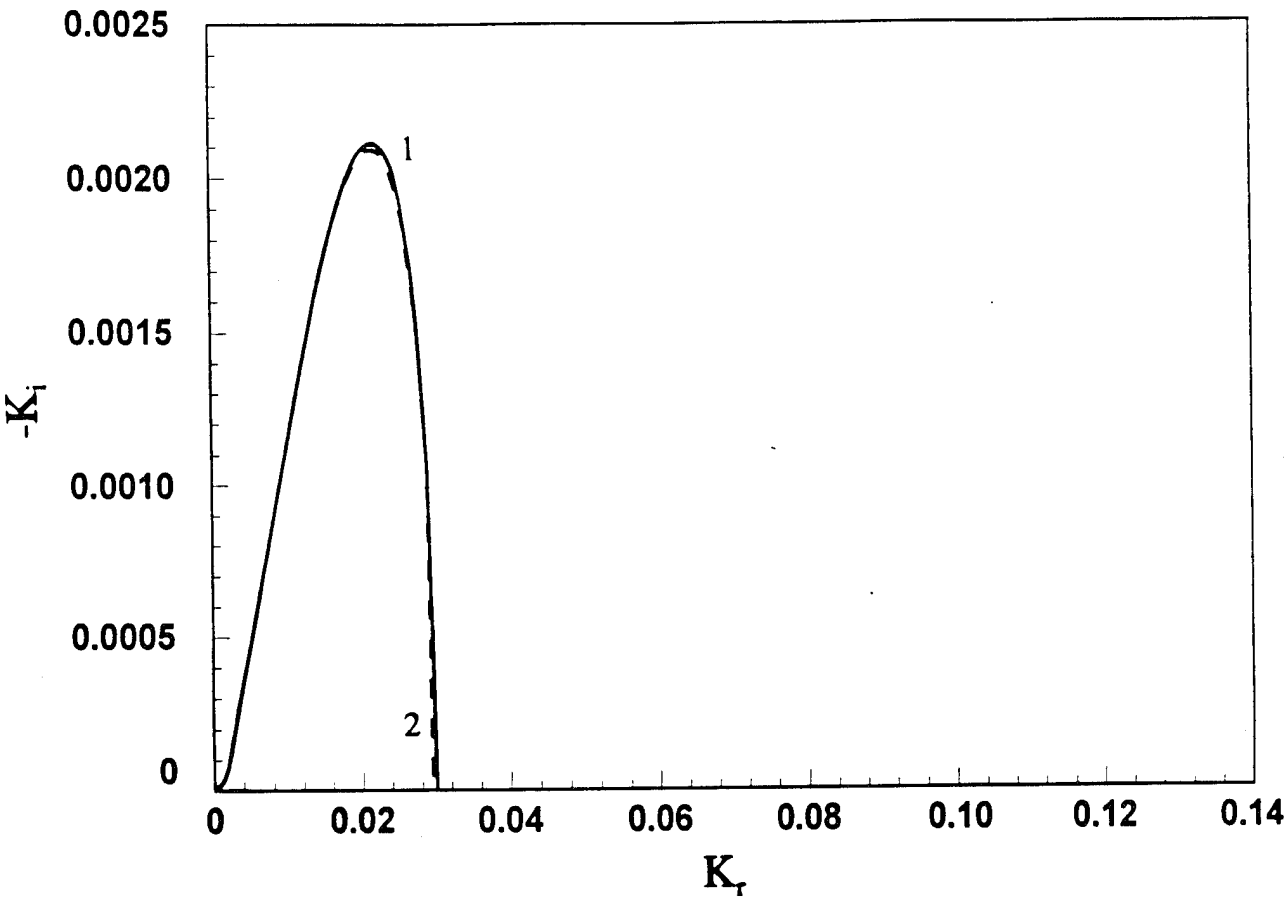

Figure 7. Aerodynamic instability of antisymmetrical disturbances. $\rho = 0.1$ and $We_g = 0.13$. Curve 1, Re = 0.25, curve 2, Re = 0.2 .

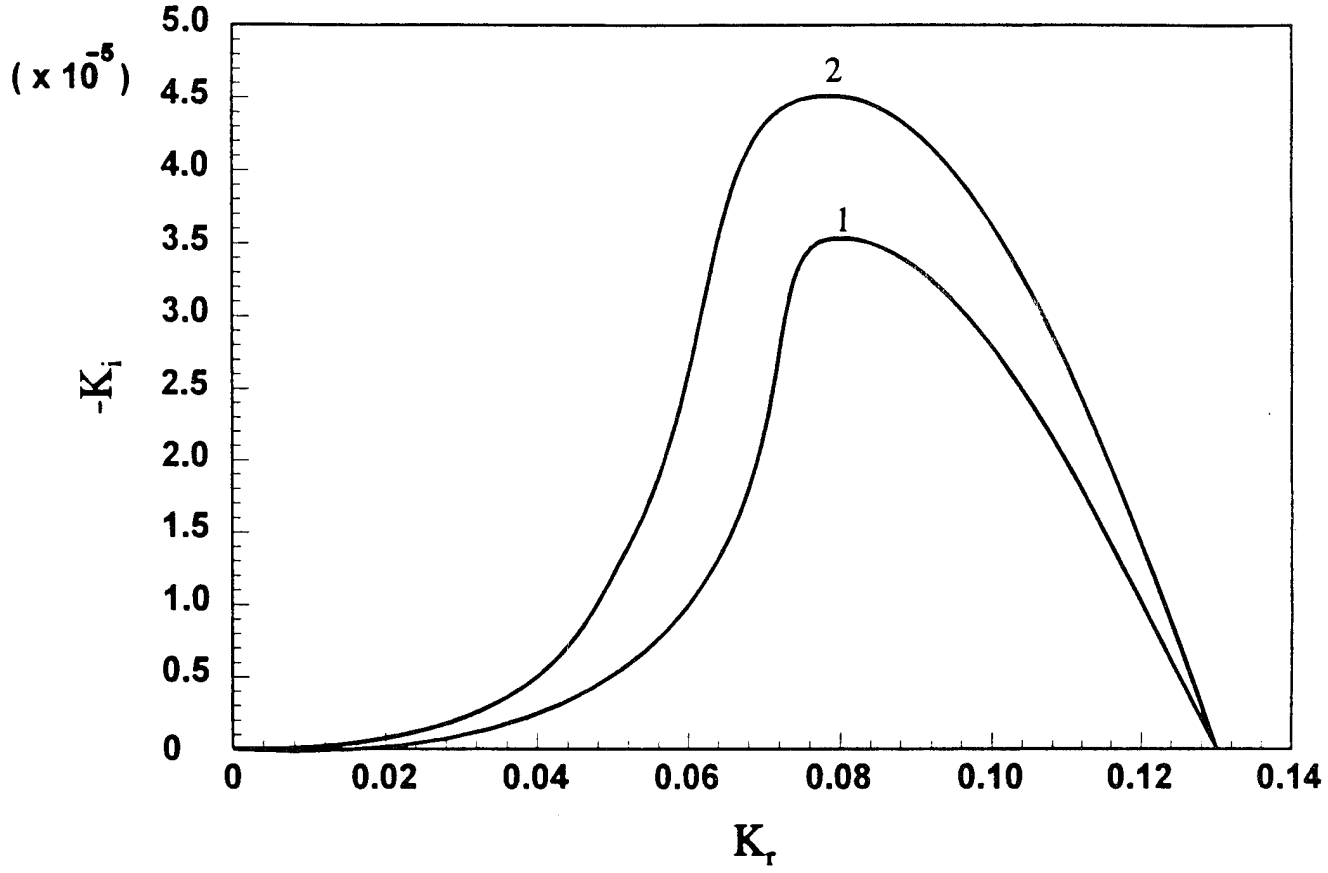

Figure 8. Viscosity-enhanced instability of antisymmetrical disturbances. ρ = 0.1 and We_g = 0.13. Curve 1, Re = 0.25 , curve 2, Re = 0.2.

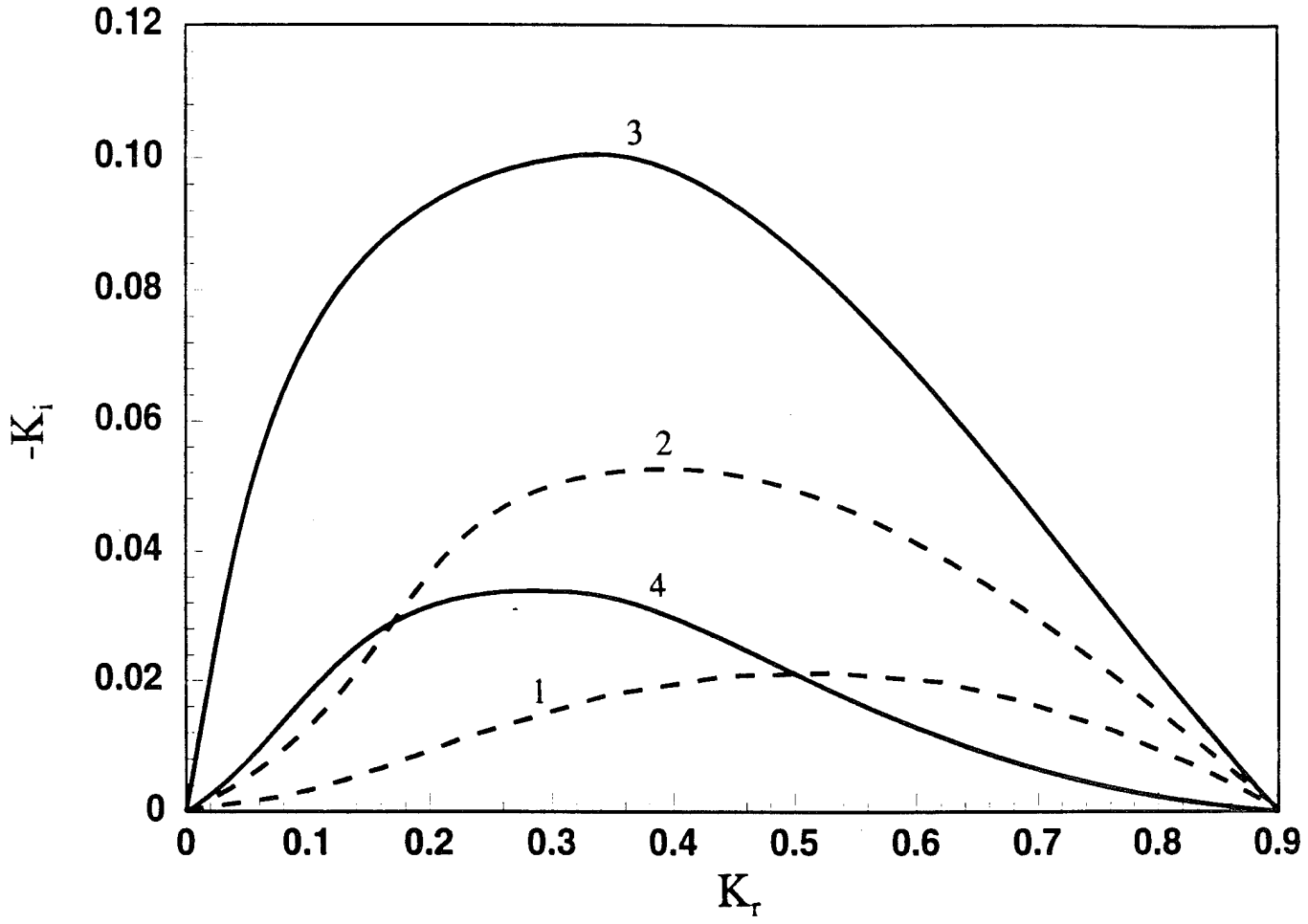

Figure 9. Effect of density ratio on instability of antisymmetrical disturbances. $We_g = 0.9$, Re = 1.0. Curve 1, $\rho = 2.0$, curve 2, $\rho = 1.0$, curve 3, $\rho = 0.1$, curve 4, $\rho = 0.01$.

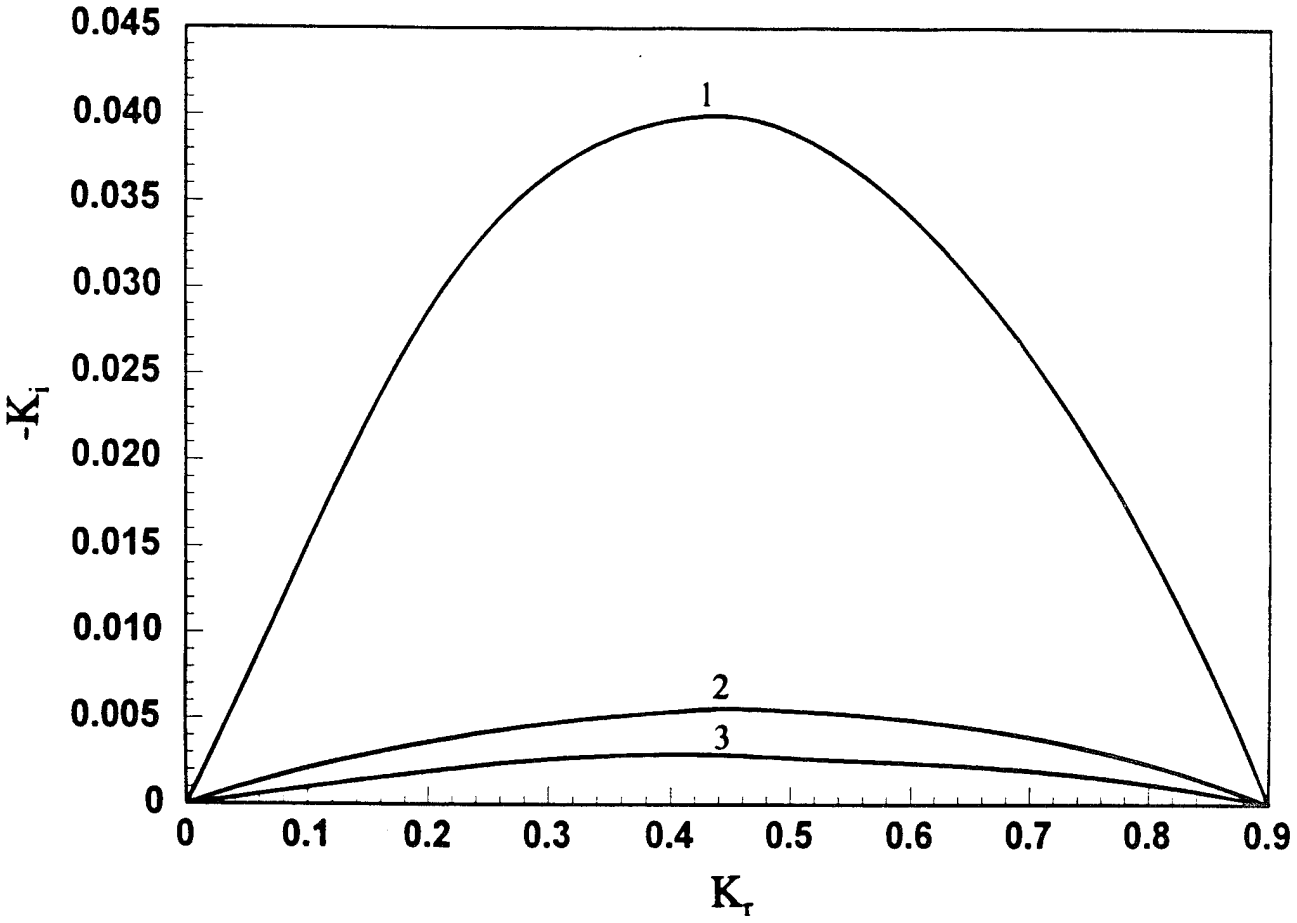

Figure 10. Effect of density ratio on instability of symmetrical disturbances. We_g = 0.9 and Re = 1.0. Curve 1, ρ = 1.0, curve 2, ρ = 0.1, curve 3, ρ = 0.05.

of instability from aerodynamic to viscosity-enhanced since the gas weber number becomes less than its critical value $We_g = \rho$. Viscosity-enhanced instability is typically associated with lower growth rates, as has been discussed earlier. For symmetrical disturbances, Fig. 10 shows that the density ratio always enhances the instability, as expected, since no critical gas Weber number exists. The present results are in general agreement with Dombrowski and Hooper's[27] experimental observations in their study of the effect of ambient density on the instability and disintegration of flat sheets.

The effect of surface tension, through the gas weber number, on the spatial instability by antisymmetrical and symmetrical disturbances is investigated in Figs. 11 and 12, respectively, for $\rho = 0.1$, Re = 1.25 and We = 0.16, 1.0, 4.0. The trend in Figs. 11 and 12 is that decreasing the gas Weber number reduces the growth rate and the instability limit and shifts the dominant wave number to a longer wavelength. This means that surface tension always acts to stabilize the liquid sheet, i. e., to damp out the disturbances. This monotonic effect of surface tension on instability is evident from Eqs. (34) and (35). Dombrowski and Fraser[26] have observed experimentally that an increase in surface tension produced a reduction in the spray angle and increased sheet breakup length.

Figure 13 shows the maximum growth rate as a function of gas Weber number for the spatial instability of a viscous liquid sheet at $\rho = 0.1$ and Re = 1.25. Figure 13a indicates that at small gas Weber number, symmetrical disturbances have a larger growth rate than antisymmetrical ones; they dominate the instability process. As the gas Weber number increases, the growth rate for both types of disturbances increases. However, that of antisymmetrical disturbances increases much faster and, above a certain gas Weber number, antisymmetrical disturbances become predominant (Fig. 13b). This is especially true at lower values of density ratios. Li and Tankin[10] have shown that for an inviscid liquid sheet the maximum growth rate for both types of disturbances approach each other when the gas Weber number becomes very large. At low gas Weber number, symmetrical disturbances of an inviscid liquid sheet prevail over antisymmetrical ones in a fashion similar to that shown in Fig. 13a. Below the critical value $We_g = \rho$, the instability of an inviscid sheet is possible only via symmetrical disturbances. Note that in Fig. 13a the maximum growth rate for antisymmetrical disturbances correspond to viscosity-enhanced instability when the gas Weber number is under the critical value $We_g = \rho = 0.1$. Above the critical value the maximum growth rate for antisymmetrical disturbances corresponds to aerodynamic instability.

Figure 14 shows the dominant wave number that corresponds to maximum growth rate for antisymmetrical and symmetrical disturbances for $\rho = 0.1$ and Re = 1.25. The dominant wave number for symmetrical disturbances is always greater than the

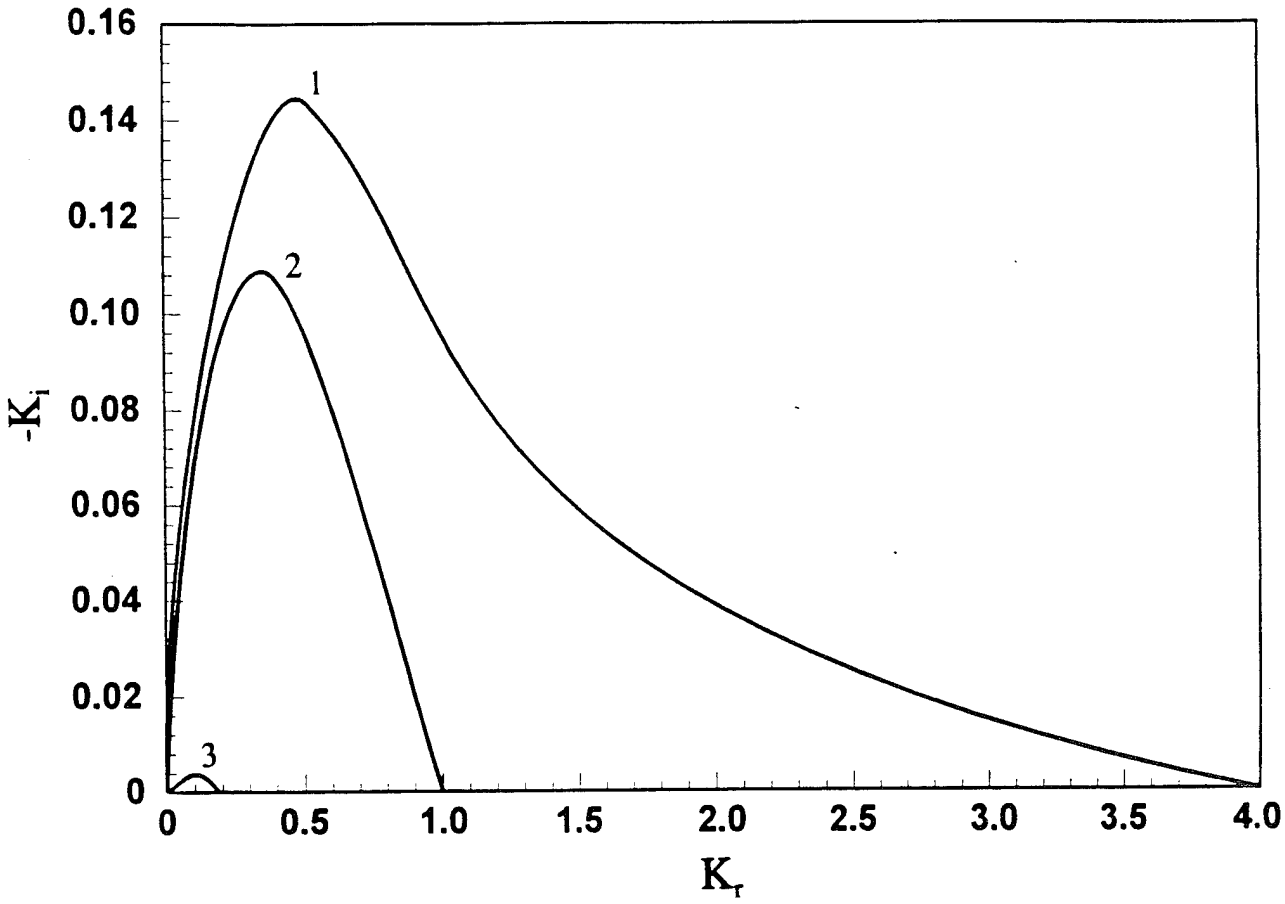

Figure 11. Effect of gas Weber number on instability of antisymmetrical disturbances. $\rho = 0.1$ and Re = 1.25. Curve 1, $We_g = 4.0$, curve 2, $We_g = 1.0$, curve 3, $We_g = 0.16$.

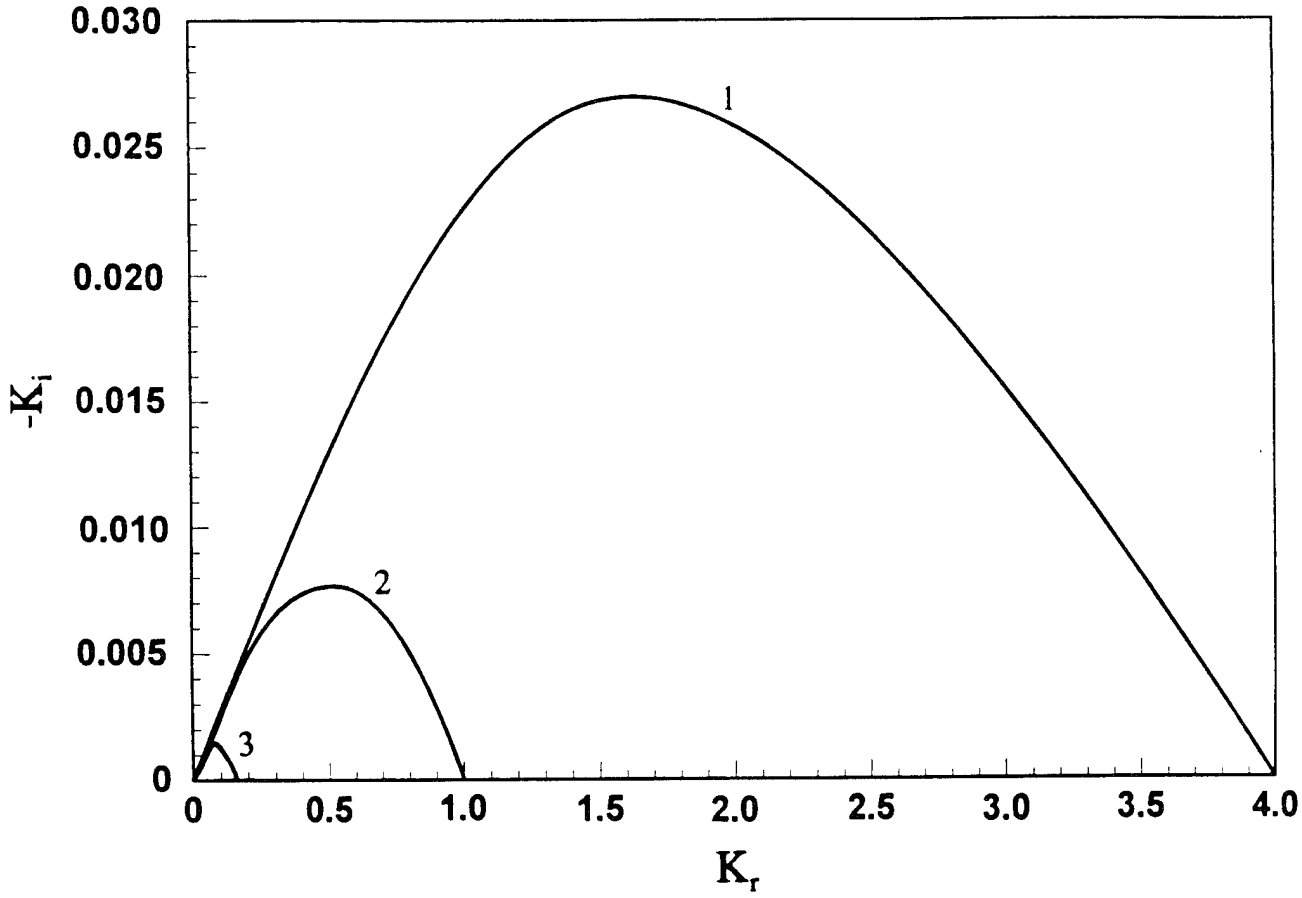

Figure 12. Effect of gas Weber number on instability of symmetrical disturbances. $\rho = 0.1$ and Re = 1.25. Curve 1, $We_g = 4.0$, curve 2, $We_g = 1.0$, curve 3, $We_g = 0.16$.

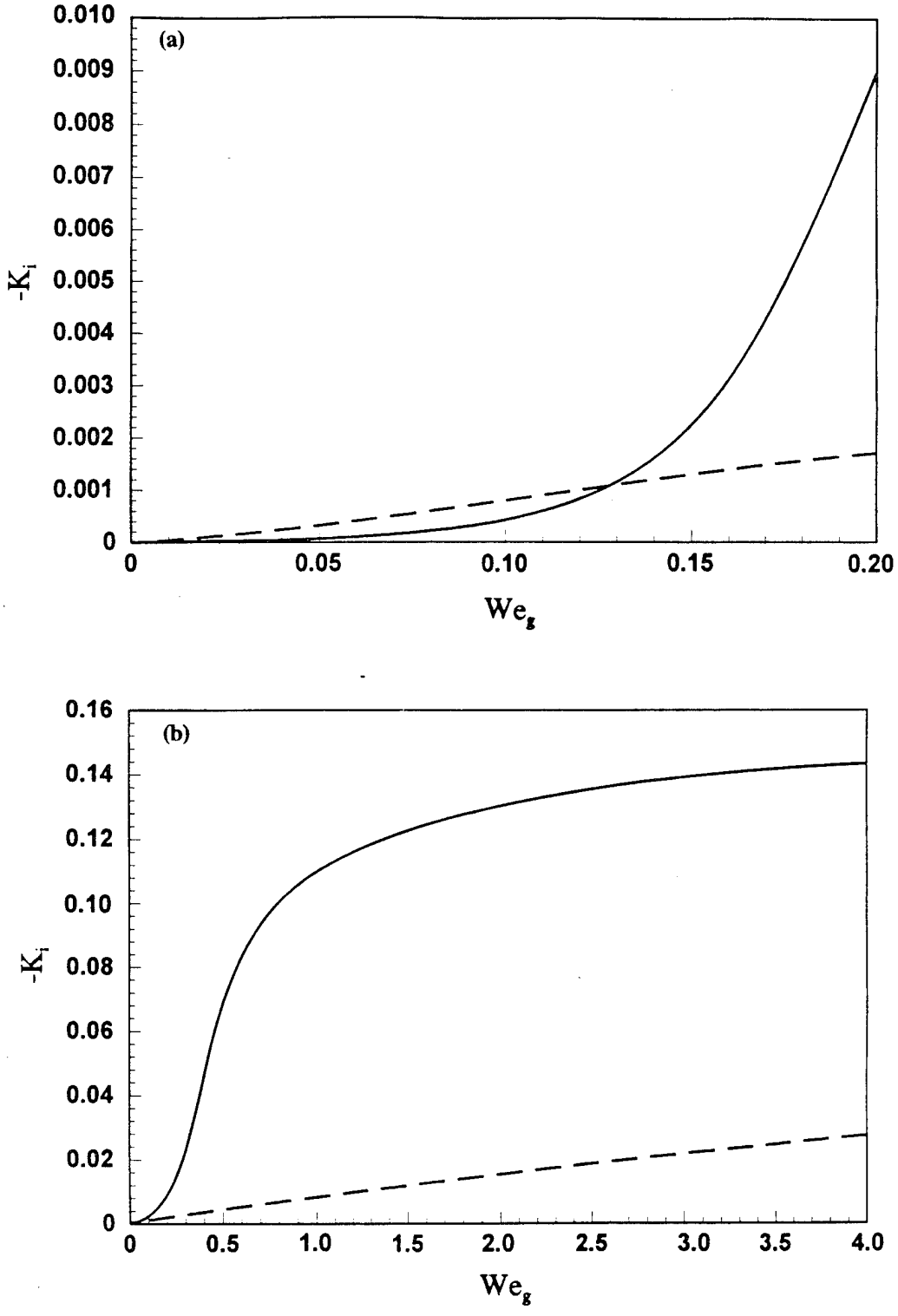

Figure 13. Maximum growth rate for a viscous liquid sheet. ρ = 0.1 and Re = 1.25. Solid curve, antisymmetrical disturbances, dashed curve, symmetrical disturbances.

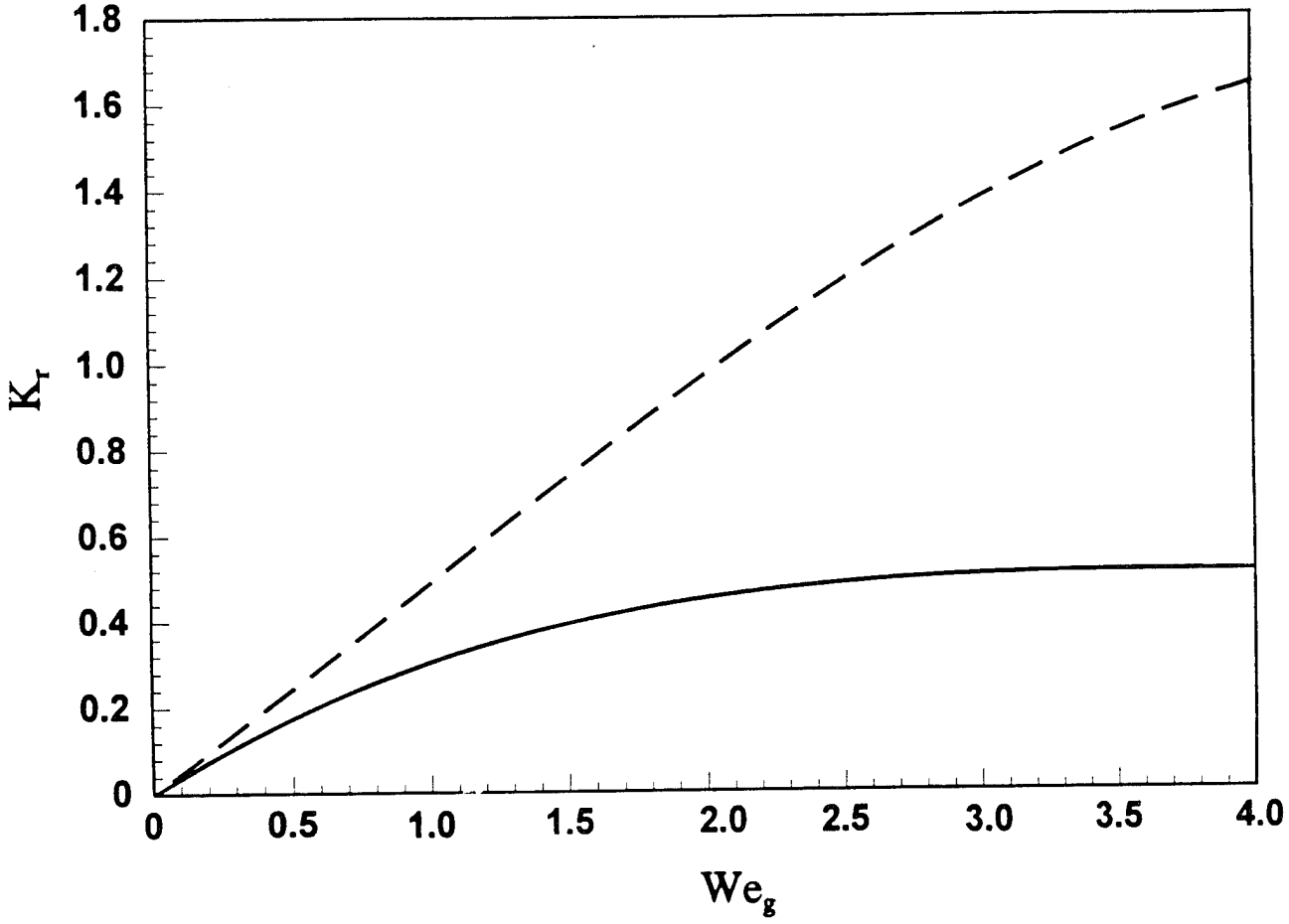

Figure 14. Dominant wavenumber for a viscous liquid sheet. ρ = 0.1 and Re = 1.25. Solid curve, antisymmetrical disturbances, dashed curve symmetrical disturbances.

corresponding value for antisymmetrical ones. Li and Tankin[10] demonstrated that for an inviscid liquid sheet, the dominant wave number of symmetrical disturbances is greater than that of antisymmetrical disturbances, except for very large gas Weber number where both types of disturbances reach asymptotically the same dominant wave number. However, for a viscous liquid sheet, the dominant wave number of symmetrical disturbances continue to increase faster than that of antisymmetrical disturbances as can be seen from Fig. 14.

CONCLUSIONS

The spatial instability of a viscous liquid sheet in an inviscid gas medium with respect to symmetrical and antisymmetrical disturbances is investigated. It is found that the growth rate and instability limit of spatial instability are always larger than those associated with temporal instability. The effects of liquid viscosity, surface tension, and gas-to-liquid density ratio on instability are reported. For a viscous liquid sheet two modes of instability coexist, namely, aerodynamic and viscosity-enhanced in contrast to inviscid liquid sheets for which the only mode of instability is aerodynamic. For symmetrical disturbances, aerodynamic instability prevails and liquid viscosity always reduces the growth rate and dominant wave number. For antisymmetrical disturbances, the relative magnitude of the gas Weber number and gas-to-liquid density ratio dictates which instability mode predominates. If the gas Weber number is large compared to the gas-to-liquid density ratio, the instability is due to aerodynamic effects. The growth rate and dominant wave number of antisymmetrical disturbances are reduced as the liquid viscosity is increased. At gas Weber numbers that are smaller than the gas-to-liquid density ratio, viscosity-enhanced instability is the only possible mode of instability, and liquid viscosity promotes instability. Increasing the gas-to-liquid density ratio raises the growth rate symmetrical and antisymmetrical disturbances. However, the gas-to-liquid density ratio reduces the growth rate of antisymmetrical disturbances if the gas Weber number falls below a critical value $We_g = \rho$, since the instability mechanism is then changed to that of viscosity-enhanced. The surface tension, effected through Weber number, always acts as a stabilizing agent. It is also found that symmetrical disturbances control the instability process for small gas Weber number, while antisymmetrical disturbances dominate for large Weber number. The dominant wave number of symmetrical disturbances is always greater than that of symmetrical disturbances. It should be noted that although the salient features of sheet instability are predictable through linear stability analysis, the results are only valid for the initial stages of sheet instability when the disturbance amplitudes are infinitesimally. A nonlinear theory is needed to accurately predict important atomization parameters such as breakup length, spray angle, and drop size.

NONLINEAR ANALYSIS

Clark and Dombrowski[11] advanced a second order perturbation analysis of the aerodynamic growth of sinuous waves on plane liquid sheets. They derived equations which describe the characteristics of the fundamental mode and the first harmonic. A solution has been obtained for the case where the wavelengths are relatively long compared with the sheet thickness. The solutions have been utilized to calculate the breakup lengths of attenuating sheets and the results were compared with measured values. However, Clark and Dombrowski[11] employed many approximations in calculating the breakup lengths, including neglecting the second order growth rate, which diminished the accuracy of their predictions. Only a pictorial representation of a sinuous wave at breakup was produced. In the present work, The theory developed by Clark and Dombrowski[11] will be used to arrive at more accurate predictions of the sheet breakup length by eliminating most of the approximations introduced by Clark and Dombrowski. The time evolution of the interfaces of liquid sheets of constant thickness as well as attenuating sheets will be studied. The size of the drops and the angle of the spray produced by the sheet breakup is computed through the nonlinear theory.

The equations of the second order perturbation solution are given by

$$\eta_j = \sum_{r=1}^{2} \eta_0^r \, \eta_{j,r} \tag{36}$$

where η_j is the surface disturbance, j = 1 corresponding to the upper and j = 2 to the lower interfaces, and η_0 is the amplitude of the initial disturbance. Therefore,

$$\eta_1 = \eta_0 \, \eta_{1,1} + \eta_0^2 \, \eta_{1,2} \tag{37}$$

$$\eta_2 = \eta_0 \, \eta_{2,1} + \eta_0^2 \, \eta_{2,2} \tag{38}$$

$\eta_{1,1}$ and $\eta_{2,1}$ are obtained from the solution of the first order equations

$$\eta_{1,1} = \eta_{2,1} = \psi_1 \exp(ikx) + \overline{\psi}_1 \exp(-ikx) \tag{39}$$

where

$$\psi_1 = \frac{1}{2} \cosh(\beta t) \exp(i\alpha t) \tag{40}$$

and the overbar indicates conjugate quantities. α and β are the real and imaginary parts of the complex wave frequency ω and its

conjugate, i.e.

$$\alpha = \frac{-Uk}{1 + \rho_g / [\rho_\ell \tanh(kh)]} \tag{41}$$

$$\beta = \frac{[\rho_\ell \rho_g U^2 k^2 \tanh(kh) - \sigma k^3 (\rho_\ell \tanh(kh) + \rho_g)]^{1/2}}{\rho_\ell \tanh(kh) + \rho_g} \tag{42}$$

where h is half the sheet thickness. $\eta_{2,1}$ and $\eta_{2,2}$ are given by the solution of the second order equations

$$\eta_{j,2} = \psi_{j,2} \exp(2ikx) + \overline{\psi}_{j,2} \exp(-2ikx) \tag{43}$$

$$\begin{aligned}\psi_{j,2} = \frac{(-1)^j k^2 \beta^2 h}{4(2\beta+\beta')(2\beta-\beta')} [\cosh(2\beta t) - \cosh(\beta' t)] \exp(2i\alpha t) \\ + \frac{k^2\beta^2 h}{4\beta^2} [\cosh(\beta' t) - 1] \exp(2i\alpha t)\end{aligned} \tag{44}$$

where β' is given by

$$\beta' = \frac{2[\rho_g \rho_\ell U^2 k^2 \coth(2kh) - 2\sigma k^3 (\rho_\ell \coth(2kh) + \rho_g)]^{1/2}}{\rho_\ell \coth(2kh) + \rho_g} \tag{45}$$

RESULTS AND DISCUSSION

Equations (36-45) are used to compute the development of the disturbance of the liquid sheet surface in time t and distance x. The flow parameters correspond to a water sheet issued in atmospheric air at room temperature (ρ_ℓ = 1000 kg/m^3, ρ_g = 1 kg/m^3, σ = 0.0728 N/m) and U = 30 m/sec. The sheet half thickness is taken as h = 2.4x10^{-4} m and the wave number k = 2000 m^{-1} so that the wavelength is $\lambda = 2\pi/k$ = 3.14x10^{-3} m. These conditions are within the range maintained in the experimental investigation of Dombrowski and Hooper.[27] The amplitude of the initial disturbance is taken to be η_0 = 0.1 h = 2.4x10^{-5} m. Clark and Dombrowski[11] measured the initial amplitude of disturbances for conical sheets and reported a value of approximately $\eta_0 = 10^{-4}$ m. They found that using η_0 = 3x10^{-4} m in their theoretical calculations of breakup length resulted in a satisfactory agreement with their measurements. It was not possible for Clark and Dombrowski[11] to measure η_0 for spray sheets since the presence of the rims precludes observations along the plane of the sheet. They postulated that η_0 for spray sheets to be in the order of molecular dimensions, i. e.,

10^{-8} m. Rangel and Sirignano[14] chose the ratio of the initial amplitude to the wavelength equal to 0.025 to ensure the proper linear behavior for small time.

Figures 15-17 depict the evolution of the liquid sheet interface at t = 1.3, 1.5, and 1.64 msec, respectively. Only the modulation of the interfaces over one wavelength ($4kx/\pi = 8$) is portrayed in Figs. 15-17 since it will be the same for all other wavelengths in accordance with the temporal analysis employed here. The vertical coordinate represents ζ/η_0, where $\zeta = \eta_j - (-1)^j h$, and j = 1 or 2 corresponds to the upper and lower interfaces, respectively. Figure 15 indicates that the sinuous character of the disturbance remains for a substantial period of time up to at least t = 1.3 msec. The modulation of the liquid sheet interface is mainly through the fundamental sinuous mode. As time advances to 1.5 msec the effect of the dilational first harmonic mode becomes apparent and the sheet diminishes in thickness at points that are half wavelength apart as shown in Fig. 16. In Fig. 17 breakup of the liquid sheet is about to occur at time t = 1.64 msec. It is clear from Fig. 17 that the sheet disintegration is due to the growth of the first harmonic. As in the case of Taylor instability the growth of the first harmonic occurs through two effects, namely, the energy addition derived solely from the fundamental and the inherent instability of the first harmonic itself when the wave number $k < \rho_g U^2/2\sigma$. At the time of rupture, the liquid sheet disintegrates into ligaments at each half-wavelength at points equal to $3/8\lambda$ and $7/8\lambda$ of the fundamental mode in accordance with the results of Dombrowski and co-workers[11, 27] and Rangel and Sirignano.[14]

In most spray applications, liquid sheets are produced by a swirl nozzle in the form of a hollow cone or by a fan spray nozzle. In both cases the sheet radius increases as it flows away and its thickness decreases with the distance from the nozzle. Dombrowski et al.[28] have shown that the thickness of an attenuating liquid sheet at any point is inversely proportional to its distance from the nozzle, and can be expressed as

$$2h = \frac{K}{x} = \frac{K}{Ut} \qquad (46)$$

where x is the distance measured from the origin and K is a thickness parameter. Clark and Dombrowski[11] argued that when an attenuating sheet is formed from a nozzle the streamlines appear to diverge from a source situated behind it. Since the distance between this 'origin' and the orifice is negligible compared with the length of the sheet[26] x can be effectively measured from the nozzle. In general, the value of the thickness parameter, K, depends on the operating conditions. Dombrowski et al.[28] conducted a thorough investigation of the effect of the flow parameters on K and found that it is slightly affected by injection pressure and tends to a constant asymptotic value for liquids of low viscosity.

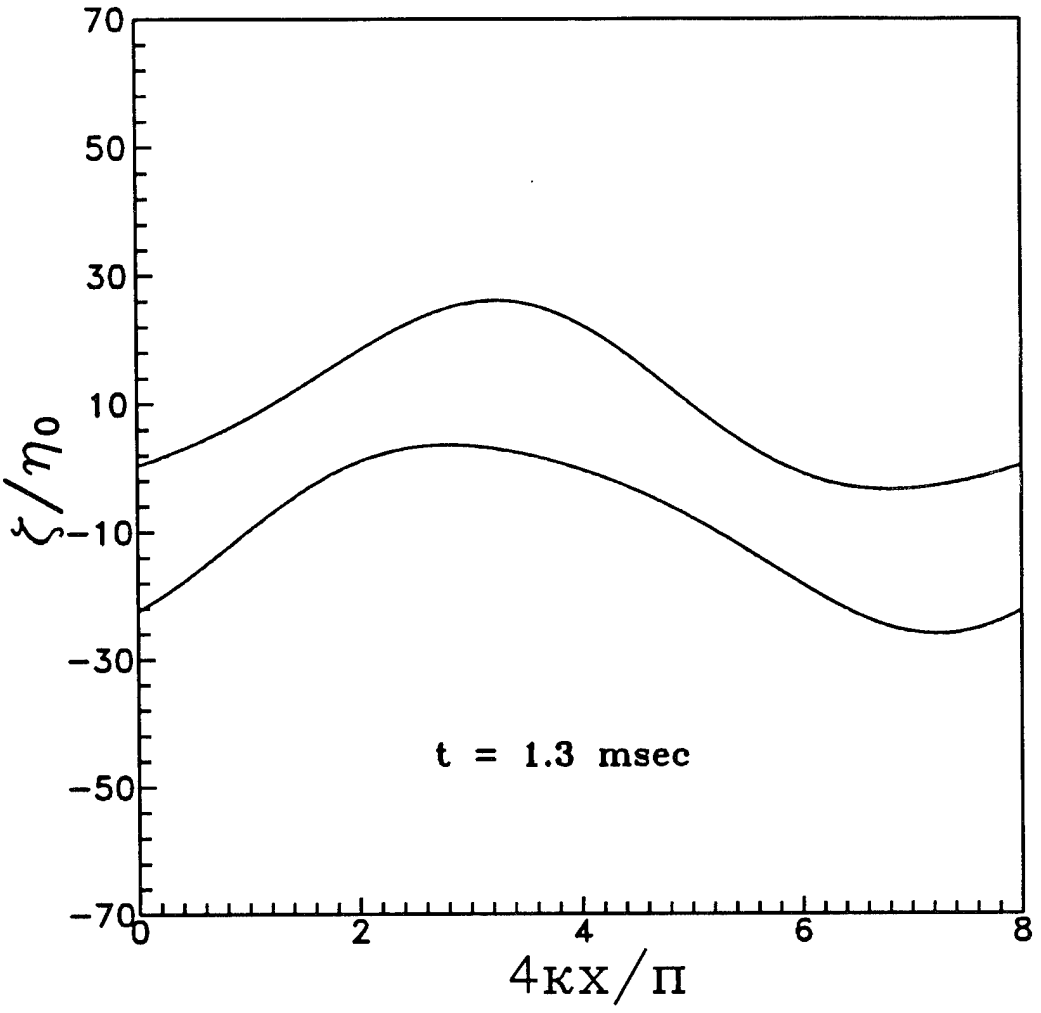

Figure 15. Interface evolution of a constant thickness liquid sheet. We = 2967, ρ = 0.001, k = 2000 m^{-1}, η_0 = 2.4x10^{-5} m, h = 2.4x10^{-4} m.

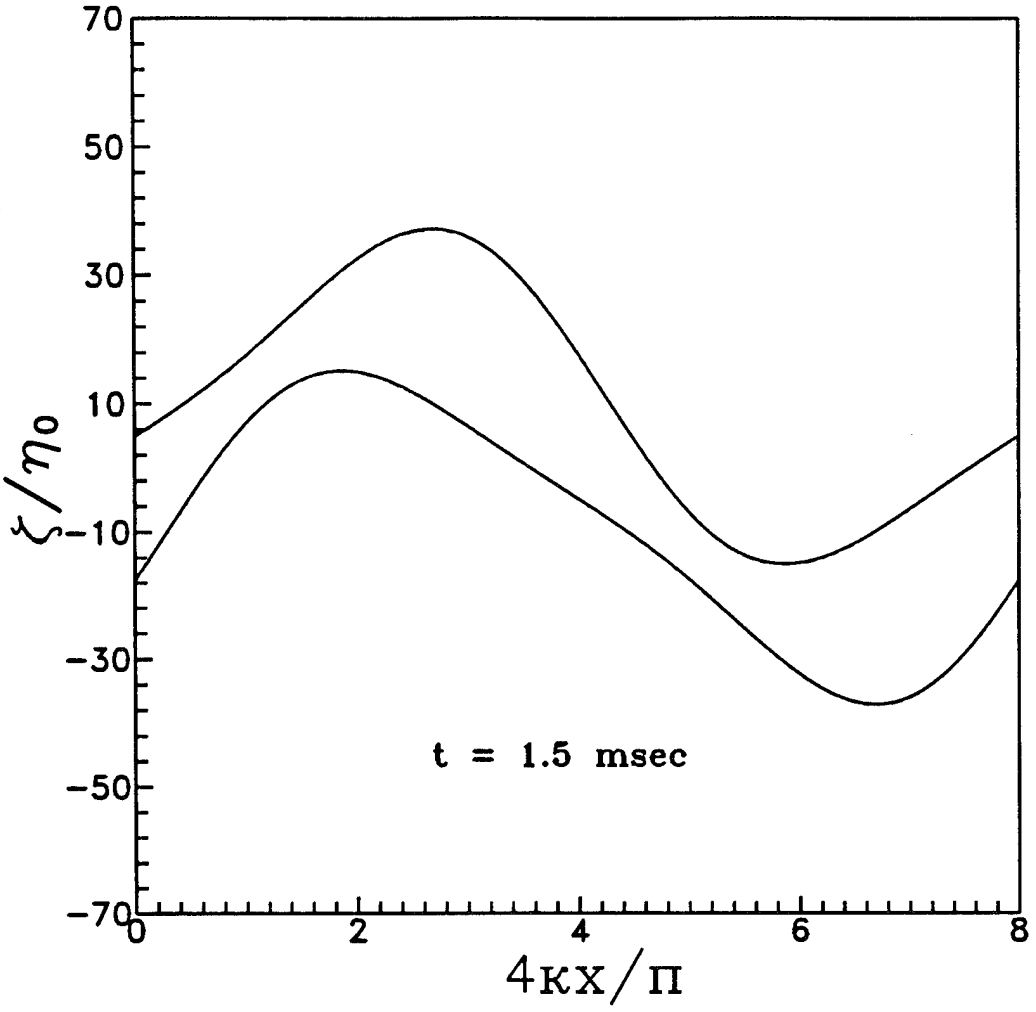

Figure 16. Interface evolution of a constant thickness liquid sheet. We = 2967, ρ = 0.001, k = 2000 m^{-1}, η_0 = 2.4x10^{-5} m, h = 2.4x10^{-4} m.

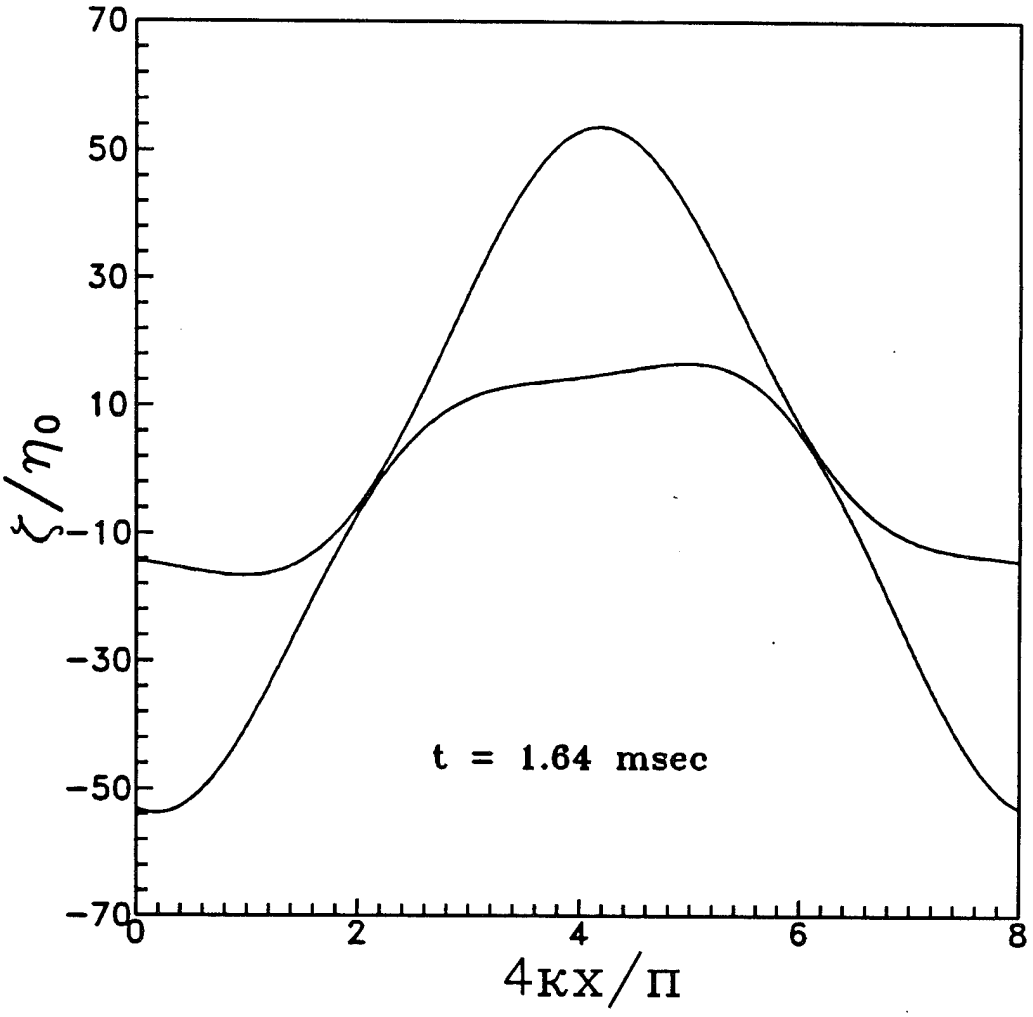

Figure 17. Interface evolution of a constant thickness liquid sheet. We = 2967, ρ = 0.001, k = 2000 m^{-1}, η_0 = 2.4x10^{-5} m, h = 2.4x10^{-4} m.

Dombrowski et al.[28] also showed that the thickness parameter, K, possesses an approximately linear relation with the orifice area. Therefore, if the thickness parameter is known for a low viscosity liquid, such as water, for a specific orifice area it could be roughly estimated for another orifice of different area.

In what follows we focus our attention on attenuating liquid sheets because of their practical importance. Figures 18-20 present three still-frames of the interfaces of an attenuating liquid sheet which delineate the various forms it assumes as time progresses up to the point of rupture. In Fig. 18 the surface disturbance is basically analogous to the fundamental sinuous wave at time t = 0.3 msec. As the time is increased to t = 0.35 msec, the effects of the first harmonic sets in and the sheet thinning becomes uneven. At t = 0.38 msec, the sheet is about to breakup and maximum thinning occurs at points interspaced by half of the wavelength of the fundamental wave. This result is similar to the case of constant thickness sheet. However, a careful comparison of Figs. 15-17 and Figs. 18-20 reveal that some major differences exist between the manner attenuating and constant thickness sheets disintegrate. First, the points of rupture of a constant thickness sheet are located at $3/8\lambda$ and $7/8\lambda$ while they are placed at $2/8\lambda$ and $6/8\lambda$ for the attenuating sheet. It is found that the location of the points of rupture varies with the flow parameters for an attenuating sheet while it is invariable for the constant thickness sheet. Nevertheless, the points of rupture remain half-wavelength apart for both constant thickness and attenuating sheets independent of other flow conditions. The thickness of the attenuating sheet at breakup is diminished by almost two orders of magnitude below that of a constant thickness sheet. This result indicates that the size of the ligaments and subsequently the drops produced by the breakup of attenuating sheets are expected to be much smaller than those of constant thickness sheets. Also, the breakup time of attenuating liquid sheets is much less than that of a sheet of constant thickness. This is expected since the attenuating sheet thickness diminishes with time. Therefore, the amplitude of the disturbance required to induce sheet breakup is smaller than for a constant thickness sheet as is evident from a comparison of Figs. 17 and 20. A smaller disturbance amplitude at breakup means less time is needed for the initial disturbance to grow.

The breakup length of an attenuating sheet may be estimated from the breakup time t_b and the relative velocity U as

$$x_b = Ut_b \tag{47}$$

where x_b is the breakup length. According to Taylor[29], the velocity U remains essentially constant since there is no means by which energy could be absorbed. Following Clark and Dombrowski[11], the breakup time is taken as the time at which

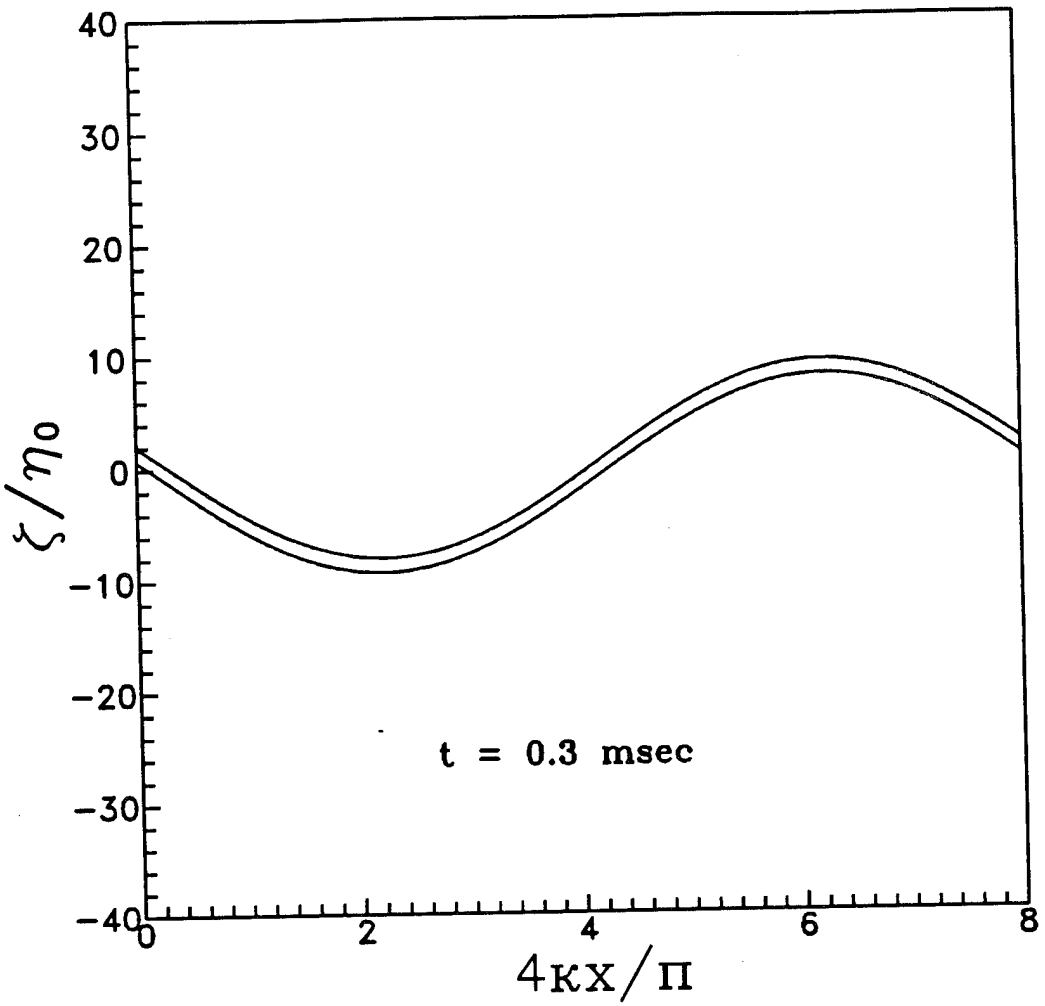

Figure 18. Interface evolution of an attenuating liquid sheet. We = 2967, ρ = 0.001, k = 2000 m^{-1}, η_0 = 2.4x10^{-5} m, h_0 = 2.4x10^{-4} m.

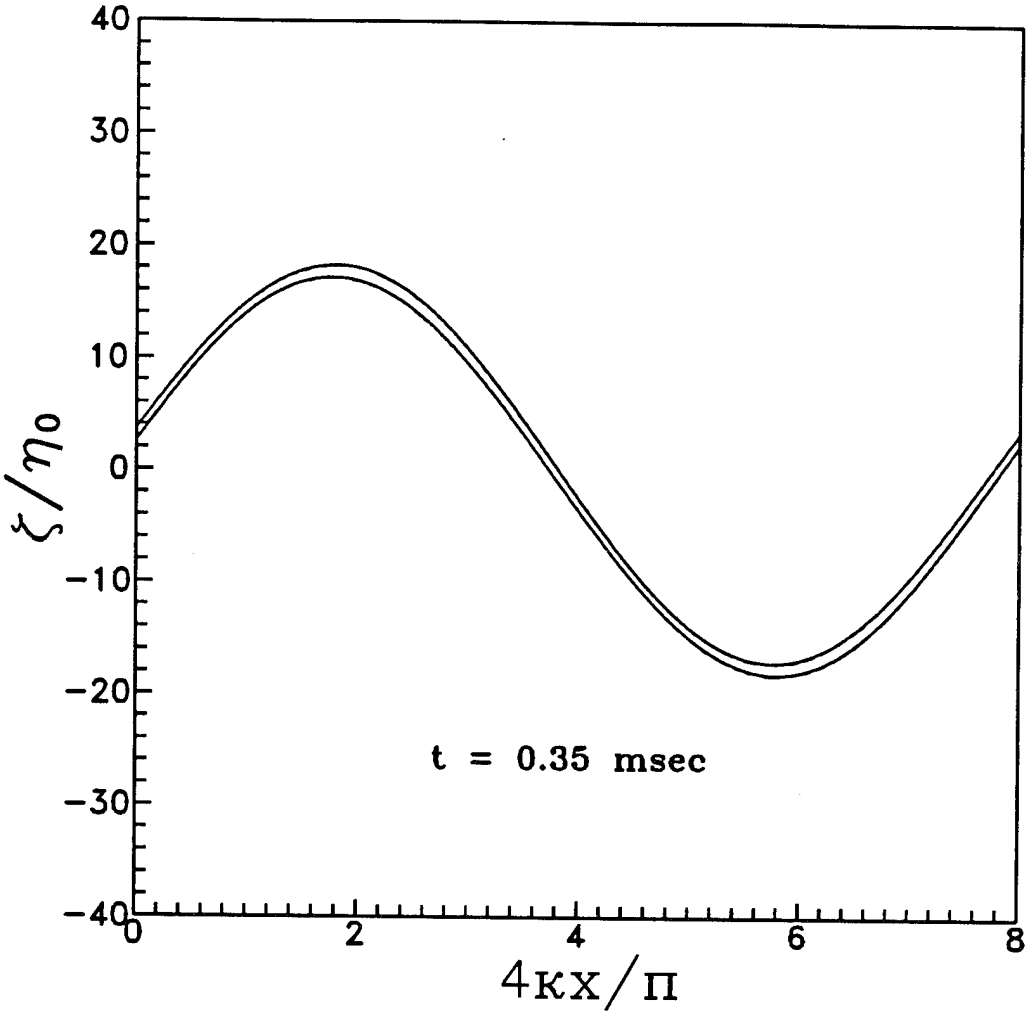

Figure 19. Interface evolution of an attenuating liquid sheet. We = 2967, ρ = 0.001, k = 2000 m^{-1}, η_0 = 2.4x10^{-5} m, h_0 = 2.4x10^{-4} m.

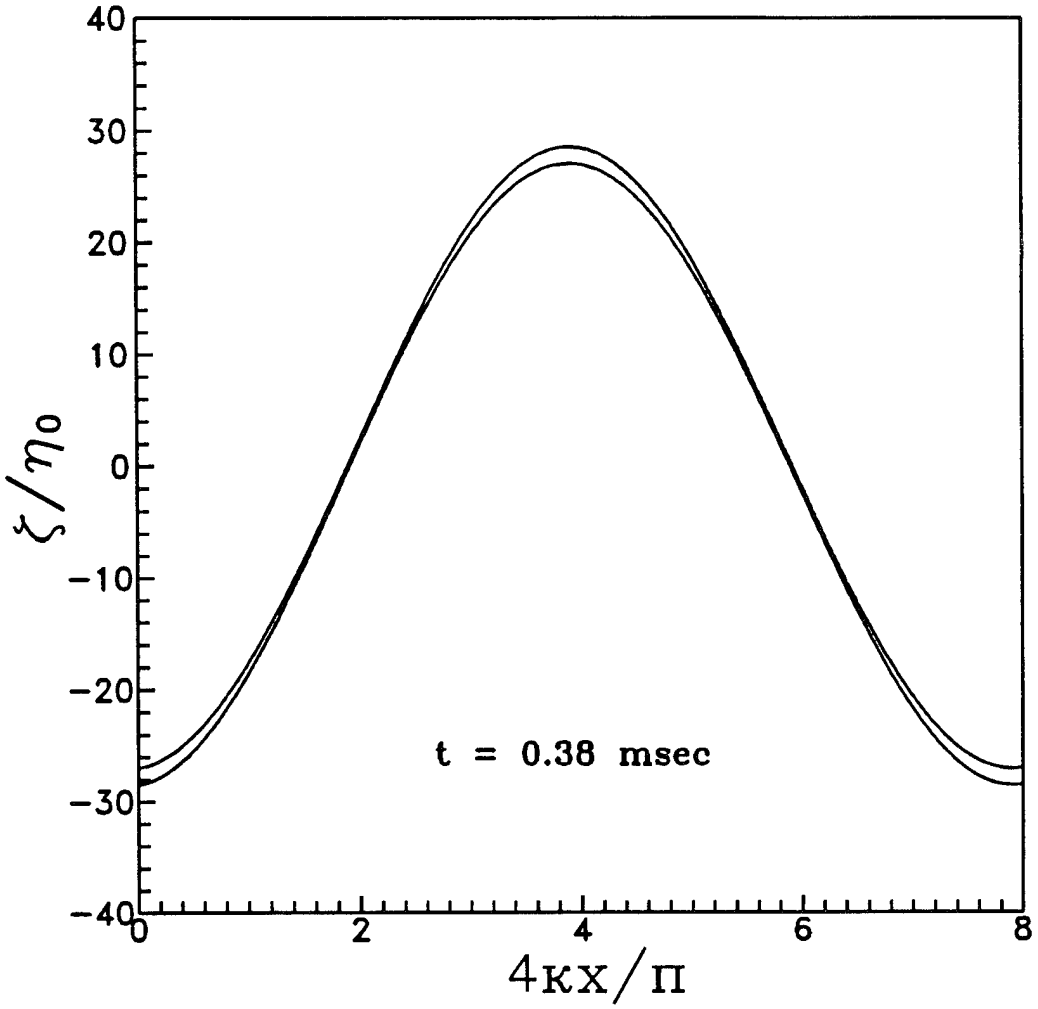

Figure 20. Interface evolution of an attenuating liquid sheet. We = 2967, ρ = 0.001, k = 2000 m^{-1}, η_0 = 2.4x10^{-5} m, h_0 = 2.4x10^{-4} m.

$$\eta_2(x_b, t_b) - \eta_1(x_b, t_b) = 2h \qquad (48)$$

where h is given by Eq. (46) for an attenuating liquid sheet. The value of the thickness parameter, K, in Eq. (46) is matched with the experimental values reported by Dombrowski and Hooper[27] to facilitate comparison. Figures 21 and 22 show such comparison of the calculated breakup lengths and the measurements of Dombrowski and Hooper[11] for the U-nozzle and W-nozzle described in their work, respectively. For both nozzles, the calculations are made for the conditions corresponding to a sheet of water injected into atmospheric air at room temperature. As mentioned earlier, k = 2000 m^{-1}, and $\eta_0 = 0.1\ h_0$ where h_0 is the initial half thickness of the attenuating sheet. For U-nozzle, $h_0 = 2.4\text{x}10^{-4}$ m, $K = 28.2\text{x}10^{-8}$ m^2, orifice area $A = 0.00448\text{x}10^{-4}$ m^2, and for W-nozzle $h_0 = 1.85\text{x}10^{-4}$ m, $A = 0.00289\text{x}10^{-4}$ m^2 , and $K = 16.5\text{x}10^{-8}$ m^2. The computations started at an initial time $t_0 = K/2h_0U$ in accordance with Eq. (46). The total duration needed for breakup is obtained by subtracting this initial time from the time at which Eq. (47) is satisfied. The initial time t_0 was found to be very small compared to the breakup time. At each time step of 1 μsec the sheet thickness is updated according to Eq. (46). and the disturbance amplitudes are computed from Eqs. (36-45) at 101 nodes over one wavelength. The relative velocity U is varied over the range of 18-30 m/sec which is within the range of the measurements performed by Dombrowski and Hooper.[27] The experimental data are computed from the empirical correlation developed by Dombrowski and Hooper[27]

$$\frac{x_b \cdot \rho}{K} = 1.5 \ln(\eta_b/\eta_0)\ We^{1/2}\ \frac{(We + 1)}{(We - 1)} \qquad (49)$$

where ρ is the gas to liquid density ratio, η_b is the amplitude of the disturbance at breakup according to the linear theory, and We is the liquid Weber number, $We = \rho_\ell U^2\ h_0/\sigma$. Dombrowski and Hooper[11] assumed that $\ln(\eta_b/\eta_0) = 12$, i. e., the same as that obtained by Weber[30] for liquid jets based on a linear stability analysis.

Figures 7 and 8 demonstrate the variation of the breakup lengths versus Weber number for U-nozzle and W-nozzle, respectively. It is observed that the predicted breakup lengths are consistently in good agreement with the values obtained from Dombrowski and Hooper's[27] empirical correlation given by Eq. (49). The predicted breakup lengths are somewhat overestimated compared to the experimental values particularly for the W-nozzle. Figures 21 and 22 indicate that the breakup length decreases as Weber number is increased, a result that has been confirmed by Dombrowski and co-workers.[11,26] The dimensionless breakup lengths for U-nozzle are less than W-nozzle as seen from Figs. 21 and 22. However, it should be remembered that the initial sheet thickness which is used to normalize the breakup length is larger for U-nozzle than W-nozzle. Therefore, when the dimensional breakup lengths are compared a

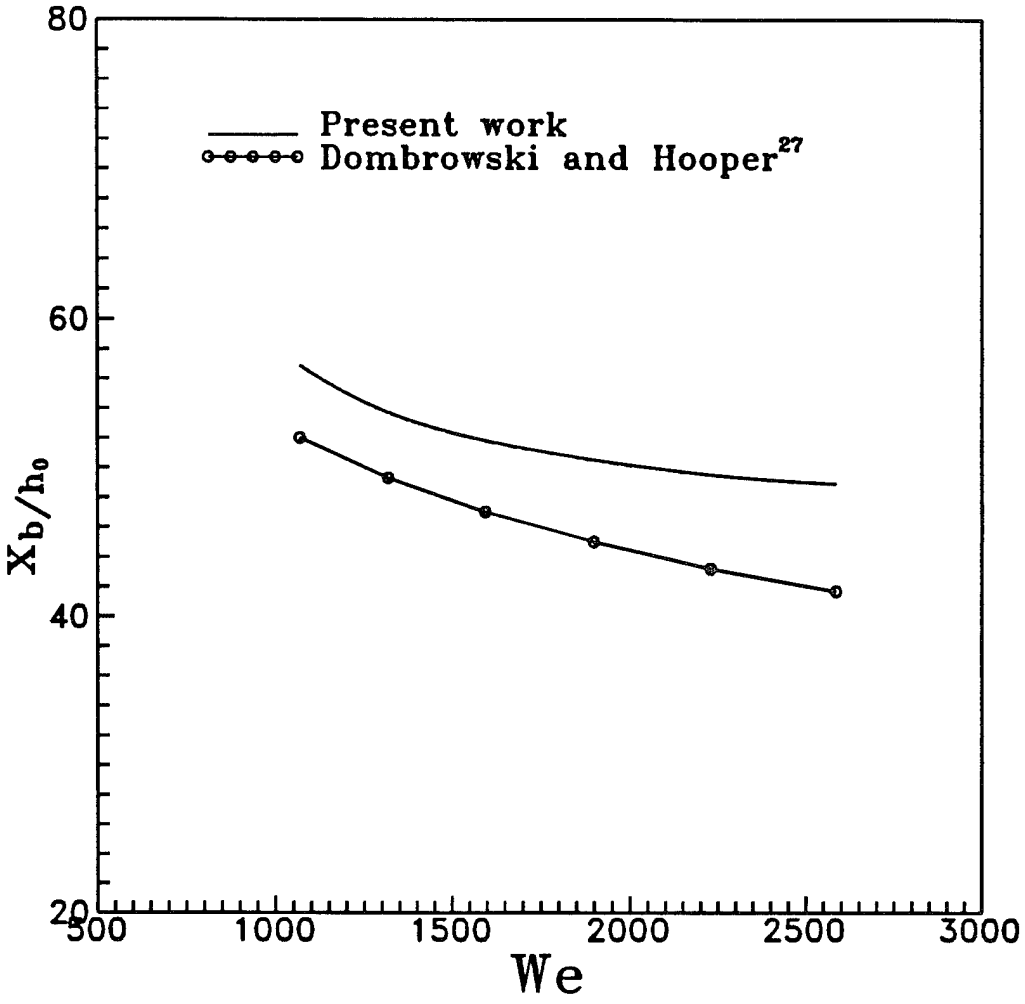

Figure 21. Variation of breakup length with We number for U-nozzle. ρ = 0.001, k = 2000 m^{-1}, η_0 = 2.4x10^{-5} m, h_0 = 2.4x10^{-4} m, K = 28.2x10^{-8} m^2.

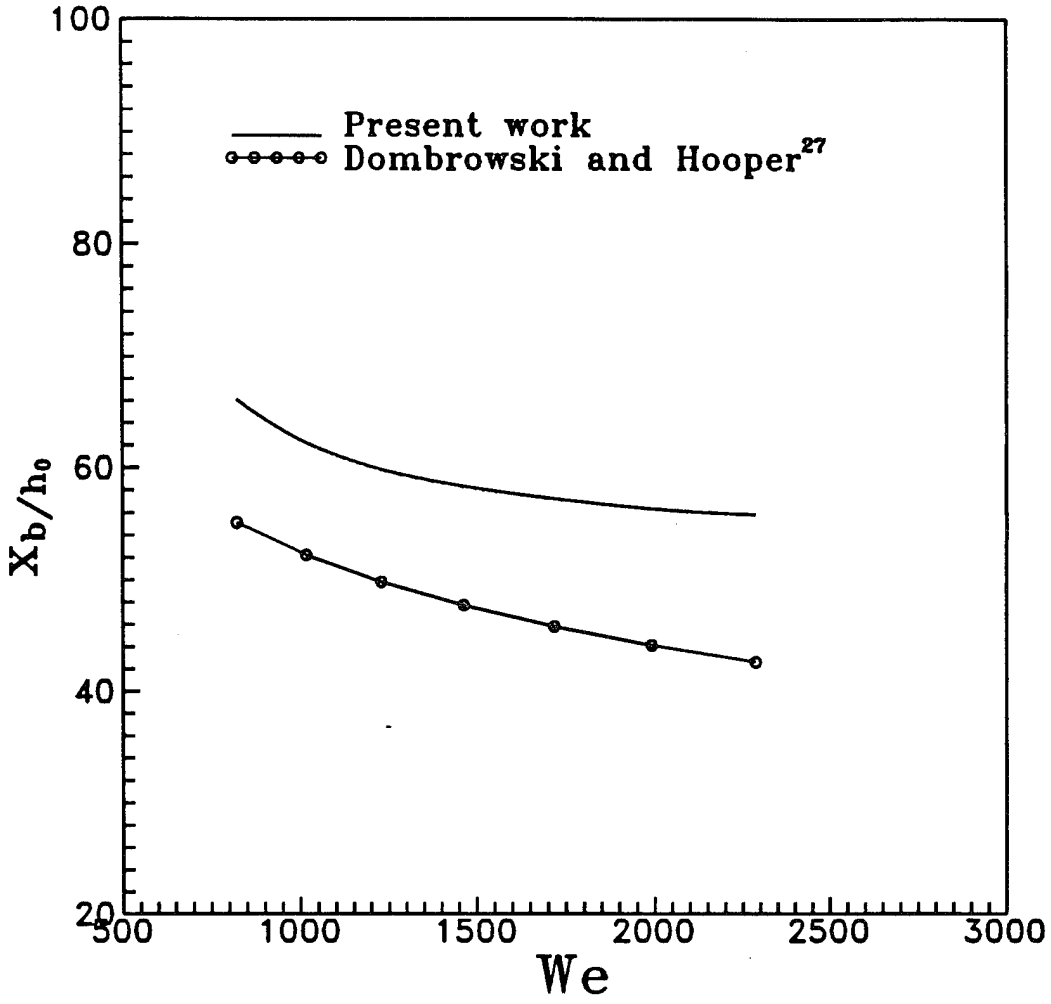

Figure 22. Variation of breakup length with We number for W-nozzle. ρ = 0.001, k = 2000 m^{-1}, η_0 = 1.85x10^{-5} m, h_0 = 1.85x10^{-4} m, K = 16.5x10^{-8} m^2.

sheet issued from U-nozzle will have a longer breakup length than a sheet emanated from W-nozzle. A longer actual breakup length is expected for U-nozzle since it has a larger initial sheet thickness. An initially thicker sheet will need to travel a longer distance over a longer period of time for its thickness to diminish to that corresponding to breakup. The longer the breakup time, the greater the breakup length at a fixed velocity in accordance with Eq. (46). It should be noted that the predictions were based on a constant wave number of k = 2000 m^{-1} which approximately represents an average value of the dominant wave number observed in Dombrowski and Hooper's[27] experimental study. No attempt was made to adjust the wave number value as Weber number is varied. This is because the wave number doesn't appear in the correlation of Dombrowski and Hooper.[27] Clark and Dombrowski[11] measured the dominant wavelengths and found that they varied linearly with Weber number. However, employing Clark and Dombrowski's[11] empirical wave number correlation would compromise the theoretical approach of the present work. It is verified that adjusting the wave number would only have a slight effect on the predicted breakup length in the range of We number investigated.

The size of drops produced by sheet breakup are of utmost importance in spray applications. Predictions of drop sizes may be obtained in the present work as follows. If $2h_b$ is the sheet thickness at breakup and k the wave number, then the diameter of the resulting cylindrical ligament that is formed at each half wavelength, as obtained by a mass balance, is given by

$$\frac{\pi}{4}D_L^2 = \frac{1}{2}\lambda.(2h_b) = \frac{\pi}{k}.(2h_b) \qquad (50)$$

where D_L is the ligament diameter. Hence,

$$D_L = \sqrt{\left(\frac{8h_b}{k}\right)} \qquad (51)$$

It has been previously observed[26] that ligaments produced from a liquid sheet contract to form liquid cylinders that move transversely in the surrounding air. The liquid cylinders then break down through symmetrical (or dilational) waves due to their interaction with the surrounding medium much as liquid jets moving in cross flow. The phenomenon of disintegration of liquid jets in cross flow has been rarely studied. The author is only aware of the work of Weihs and Frankel[30] who studied the stability of a liquid cylinder in cross flow at low Weber number. However, their results are not directly applicable in the present work since Weber number is much too large for their analysis to be valid. Dombrowski and Johns[9] postulated that the surrounding atmosphere will have no effect on the wavelength and assumed that Weber's[31] results for surface tension break down may be applied. In the present work we

adopt the more advanced theory of Lin and Lian[4] in estimating the dominant wave number, n, that corresponds to ligaments breakup. Lin and Lian[4] identified two breakup regimes of liquid jets which they termed Rayleigh (capillary) and Taylor (atomization) modes. Lin and Ibrahim[5] discovered a criterion for predicting the liquid jet breakup mode. If We < $1/\rho$ the jet breakup is due to capillary pinching and the size of the resultant drops will be of the same order as the jet radius. For We > $1/\rho$ the jet disintegrates into drops much smaller than its radius by the atomization mode. The range of We number in the present work belongs mostly to Taylor mode. In general, the dominant wave number, n, of liquid jet breakup is different than, k, the wave number corresponding to liquid sheet breakup. If it is assumed that the waves grow on the jet surface until they have an amplitude equal to the radius of the ligament, one drop will be produced per wavelength. Thus by mass balance the relation between drop size and wave number is given by

$$\frac{4}{3}\pi d_m^3 = \frac{2\pi}{n} \cdot \frac{\pi}{4} D_L^2 \qquad (52)$$

where d_m is mean drop diameter. Upon substitution from Eq. (51) into Eq. (52) we get

$$d_m = \left(\frac{3\pi h_b}{k.n} \right)^{1/3} \qquad (53)$$

Hasson and Mizrahi[32] correlated their measurements of surface-volume mean drop diameters of sprays by

$$d_m = 0.071 \left(\frac{K^2\ \sigma^2\ \mu_\ell}{\rho_\ell\ U^2} \right)^{1/6} \qquad (54)$$

where c.g.s units are employed.

Figures 23 and 24 display a comparison of the predictions of the drop size with the empirical correlation of Hasson and Mizrahi.[32] It is observed that the predictions of mean drop diameter agree well with the experimental data. Both theory and experiment predict a decrease in the mean drop diameter as Weber number is increased. Since the breakup length decreases with Weber number then the attenuating sheet thickness at breakup, $2h_b$, is larger at higher Weber number. However, the dominant wave number of liquid jet breakup, n, increases with We number at a faster rate than h_b resulting in a reduced drop size as an examination of Eq. (53) reveals. The predicted drop size are somewhat underestimated when compared with the empirical values. This trend is consistent with that of overestimated breakup lengths discussed in conjunction with the results shown in Figs. 21 and 22. If the present computations overpredict the breakup length then the thickness of the sheet at

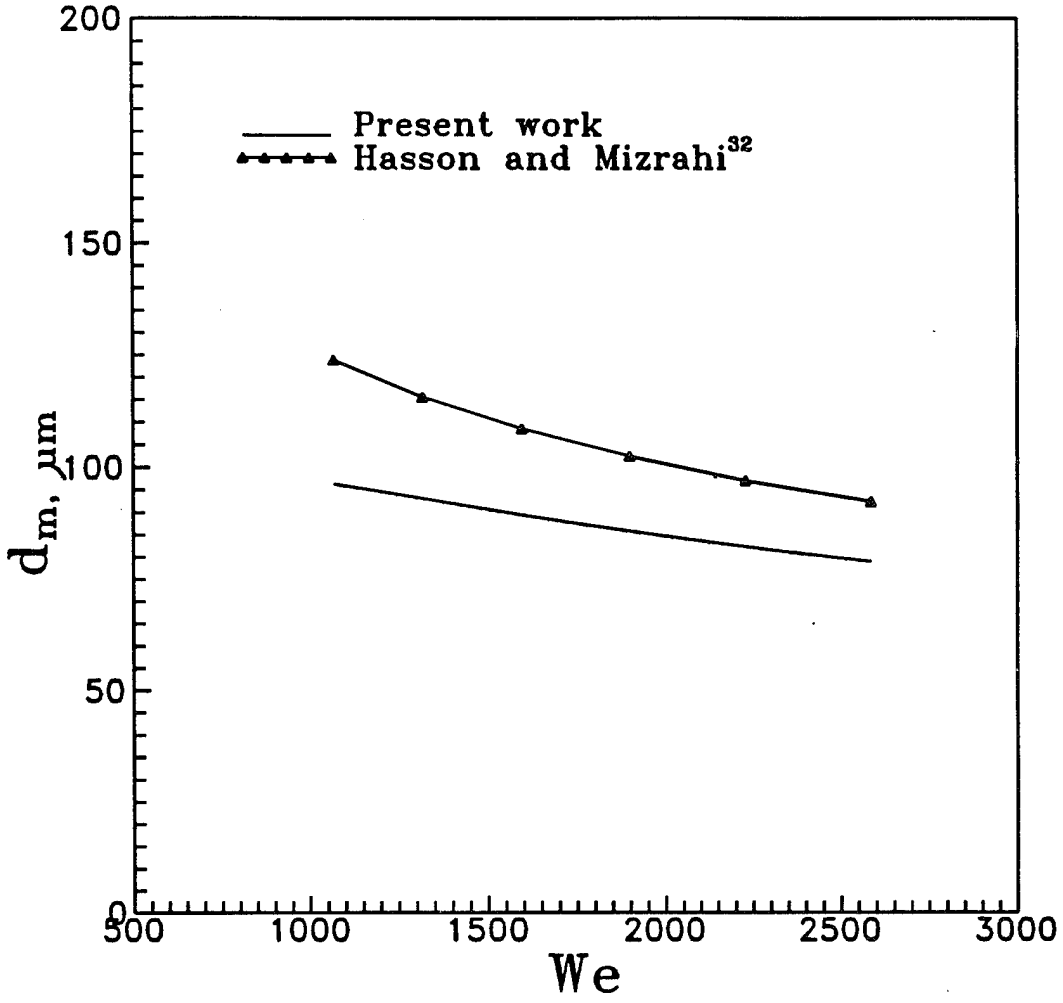

Figure 23. Variation of drop diameter with We number for U-nozzle. ρ = 0.001, k = 2000 m^{-1}, η_0 = 2.4x10^{-5} m, h_0 = 2.4x10^{-4} m, K = 28.2x10^{-8} m^2.

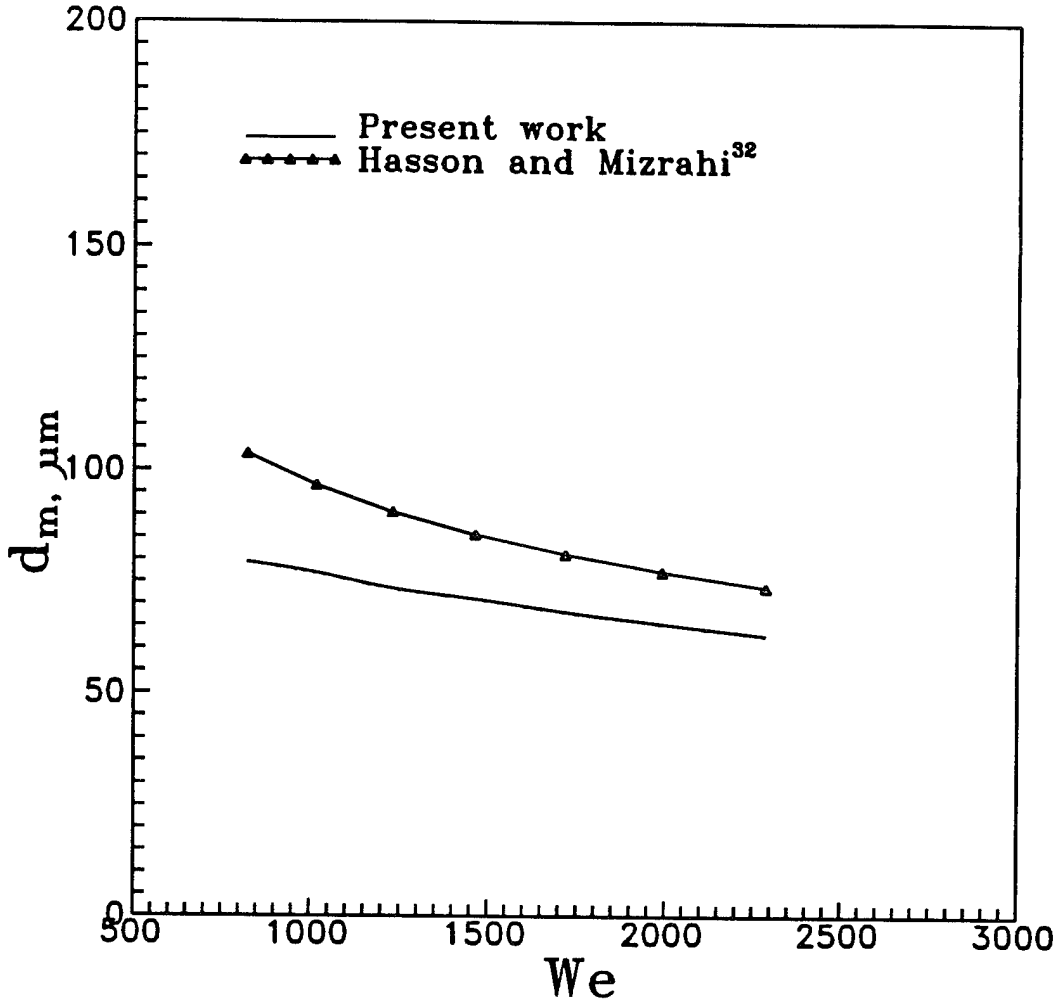

Figure 24. Variation of drop diameter with We number for W-nozzle. ρ = 0.001, k = 2000 m^{-1}, $\eta_0 = 1.85 \times 10^{-5}$ m, $h_0 = 1.85 \times 10^{-4}$ m, $K = 16.5 \times 10^{-8}$ m^2.

breakup would be thinner than it should. A smaller sheet thickness at breakup would lead to underestimating the drop size as can be seen in Eq. (53). The agreement between the theoretical and experimental drop size improves as Weber number increases. It is thought that the implementation of a theory that accurately accounts for the breakup of a liquid jet in cross flow at high We number would yield improvements in the predictions. The size of drops produced by the breakup of constant thickness sheets are larger than that produced by attenuating liquid sheets with the same initial thickness as may be confirmed by a comparison of Figs. 17 and 20.

Measurements and predictions of spray angles are rare in the literature especially for a liquid sheet. The present theory can be used to estimate the spray angle ϕ of an atomizing sheet. The spray angle may be defined as the ratio of the disturbance amplitude increase to the distance traveled by the fluid particle in the same time period. Therefore, the spray angle for a disintegrating liquid sheet is given by the ratio of the maximum amplitude of disturbance to the breakup length, i. e.,

$$\tan(\phi/2) = \frac{|\zeta_{max}|}{x_b} \qquad (55)$$

Figure 25 shows the computed values of the spray angle for U-nozzle and W-nozzle. It is seen that the spray angle increases with Weber number. As mentioned earlier Dombrowski and Fraser[26] observed a reduction in the spray angle as surface tension is increased. Therefore, the present behavior of the spray angle is in qualitative agreement with Dombrowski and Fraser's experimental results. Figure 25 demonstrates that the spray angle for U-nozzle is uniformly smaller than for W-nozzle. This is not surprising since the breakup length is larger for U-nozzle. Since the breakup length appears in the denominator of Eq.(55) a smaller spray angle would be expected when the breakup length is larger. The variations in the numerator of Eq. (55) are much smaller than the difference in the breakup length between U-nozzle and W-nozzle. Since a sheet of constant thickness would have a longer wavelength than its attenuating counterpart, the spray angles associated with constant thickness sheets are smaller than attenuating ones. The growth of the spray angle with We number slows down when We number becomes large.

The effect of Weber number on attenuating sheets breakup thickness and time for both U- and W-nozzles are demonstrated in Figs. 26 and 27, respectively. It can be observed that while the breakup thickness increases, the breakup time decreases as Weber number is increased. At high We number the sheet breaks down faster at a shorter breakup length. Therefore, the sheet thickness has less time to attenuate and the leading edge of the sheet will exhibit a

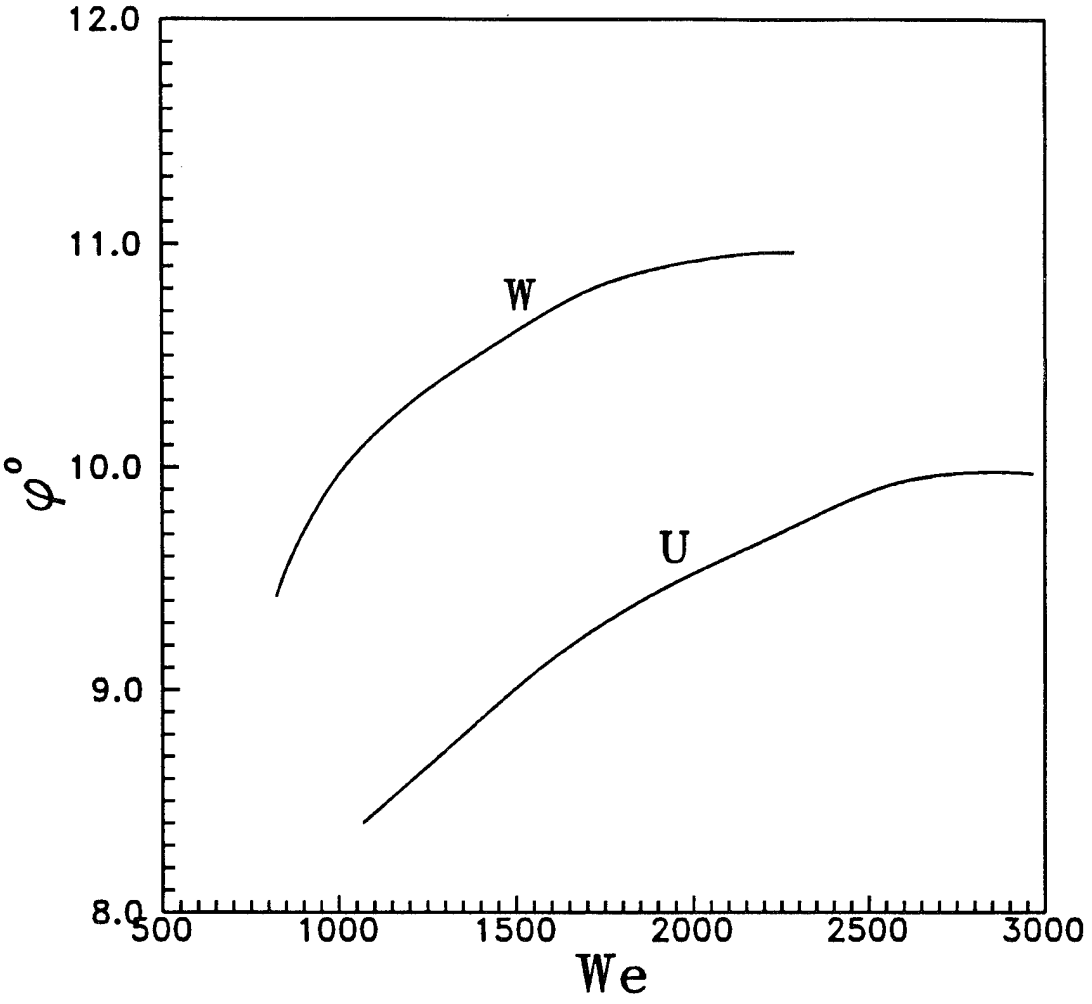

Figure 25. Spray angle variation with We number at ρ = 0.001 and k = 2000 m^{-1}. U-nozzle: η_0 = 2.4x10^{-5} m, h_0 = 2.4x10^{-4} m, K = 28.2x10^{-8} m^2. W-nozzle: η_0 = 1.85x10^{-5} m, h_0 = 1.85x10^{-4} m, K = 16.5x10^{-8} m^2.

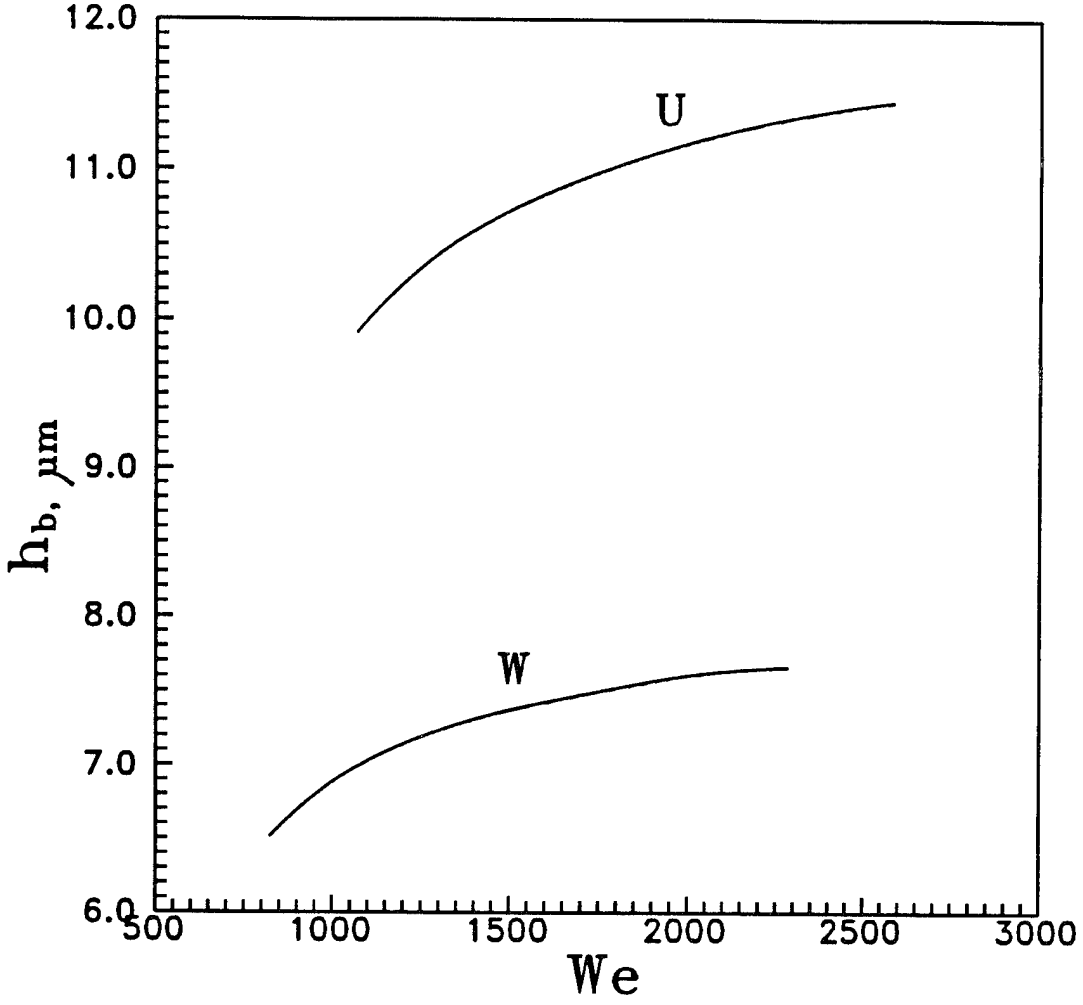

Figure 26. Sheet breakup thickness variation with We number at ρ = 0.001, k = 2000 m^{-1}. U-nozzle: η_0 = 2.4x10^{-5} m, h_0 = 2.4x10^{-4} m, K = 28.2x10^{-8} m^2. W-nozzle: η_0 = 1.85x10^{-5} m, h_0 = 1.85x10^{-4} m, K = 16.5x10^{-8} m^2.

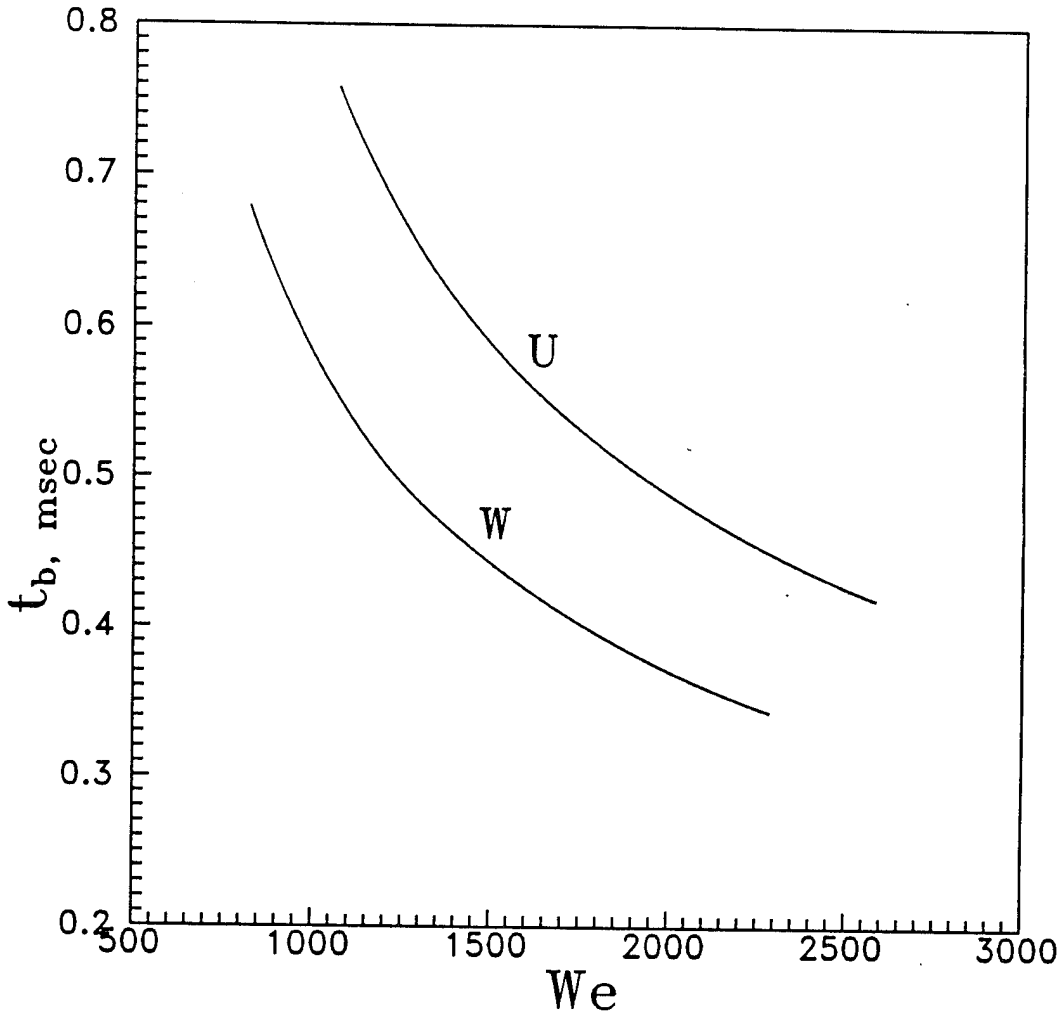

Figure 27. Sheet breakup time variation with We number at ρ = 0.001 and k = 2000 m^{-1}. U-nozzle: η_0 = 2.4x10^{-5} m, h_0 = 2.4x10^{-4} m, K = 28.2x10^{-8} m^2. W-nozzle: η_0 = 1.85x10^{-5} m, h_0 = 1.85x10^{-4} m, K = 16.5x10^{-8} m^2.

larger thickness. Both the breakup thickness and time for U-nozzle are larger than W-nozzle at any given We number since the U-nozzle has a higher initial thickness. The breakup thickness of a constant thickness sheet will be the same as its initial thickness but the breakup time is shortened as We number is raised.

The phenomenon of bi-modal atomization, in which drops of two predominant sizes are produced by the sheet breakup, may be explained in light of the present results. The possibility that bi-modal atomization occurs due to the formation of satellite drops between the main drops as in the case of liquid jet breakup[3] is ruled out. The present results indicate clearly that the sheet disintegrates into ligaments of equal size equivalent to half-wavelength of the fundamental wave. There is no evidence of satellite drops at the point of rupture as Figs. 17 and 20 would show. The hypothesis that bi-modal atomization could be a result of sheet breakup by a combination of sinuous and dilational disturbances that grow at approximately the same rate is also dismissed. As the results of the present linear analysis indicate, sinuous instability waves grow faster than dilational ones under most practical conditions.

Some forms of bi-modal atomization have been reported earlier by Dombrowski and Fraser[26], Hasson and Mizrahi[32] and Mansour and Chigier[33] among others. These studies suggest that, in bi-modal atomization, some drops are formed from the rims (or side edges) of the spray sheet which are coarser than the drops produced from the center of the spray. Mansour and Chigier[33] have observed that, under certain conditions, the sheet breakup will be due to the formation of "cell" structures. These structures are bounded by large diameter ligaments containing thin membranes inside. The ligaments are the origin of the large drops in the spray and the membranes contribute to the formation of the smaller drops. These observations agree with the results of the present nonlinear theory. The drops formed from the side edges which are thick, because their breakup length is short, would be larger than the drops produced from the center of the sheet which is thinner. In the case of breakup due to "cell" structures formation, then the thick ligament produce larger drops than the thin membranes.

CONCLUSIONS

The nonlinear calculations show similarities and dissimilarities between the manners in which a sheet of constant thickness and an attenuating sheet will breakup. It is found that the disturbance growth corresponds to a combination of a basic sinuous mode and a dilational first harmonic. As a result wave growth is asymmetric and the sheet progressively diminishes in thickness. Thinning of the sheets is caused by the growth of the harmonic waves. The sheets breakup into ligaments of half-wavelength size. However, an attenuating sheet will disintegrate faster and at a smaller

thickness than a constant thickness one. As a result, the size of the drops produced by an attenuating sheet will be smaller and the spray angle will be larger than for a constant thickness sheet of the same initial thickness.

The predicted spray characteristics of attenuating sheets compare favorably both qualitatively and quantitatively, with empirical correlations and experimental data. It is observed that the breakup lengths and mean drop diameters are reduced when Weber number increases. The spray angle slowly increases as We number is raised. The breakup thickness increases while the breakup time decreases with an increase in We number. A larger initial sheet thickness will cause the breakup length, the drop size, and both the thickness and time at breakup to increase. However, the spray angle is smaller for an attenuating sheet of larger initial thickness.

Only the sinuous breakup mode of the sheet is considered in the nonlinear computations. This is because the results of the linear theory consistently predict the dominance of sinuous waves over dilational ones unless We is smaller than the density ratio. Since in most atomization applications We number is large, restricting our study to sinuous mode is therefore justified. Dilational breakup may become important at supercritical conditions[14], however, and a study of this breakup regime has its own merits. Only temporal instability is considered in the present nonlinear analysis since it has been demonstrated that both temporal spatial instability yield approximately the same results in the high We number range investigated.[34] Finally, it is suggested that the predictions of drop size may be improved by utilizing a theory that deals directly with the breakup of liquid jets in cross flow at high We number. Therefore, the development of such a theory is warranted.

PUBLICATIONS

Ibrahim, E. A., "Spatial Instability of a Viscous Liquid Sheet," Journal of Propulsion and Power, Vol. 11, No. 1, January 1995, pp. 146-152.

Ibrahim, E. A., "Prediction of the Characteristics of the Spray Formed by Liquid Sheet Atomization," to be submitted to Journal of Engineering for Gas Turbines and Power.

PRESENTATIONS

Ibrahim, E. A., "Spatial Instability of a Viscous Liquid Sheet," presented at AIAA 32nd Aerospace Sciences Meeting and Exhibit, Reno, Nevada, January 10-13, 1994.

REFRENCES

[1]Rayleigh, L. *The Theory of Sound*, Dover, New York, 1945, p. 351.
[2]Taylor, G. I., "Generation of Ripples by Wind Blowing," *The Scientific Papers of G. I. Taylor*, Vol. 3, No. 25, Cambridge Univ. Press, Cambridge, England, UK, 1963, pp. 244-254.
[3]Bogy, D. B., "Drop Formation in a Circular Liquid Jet," *Annual Review of Fluid Mechanics*, Vol. 11, 1979, pp. 207-228.
[4]Lin S. P., and Lian, Z. W., "Mechanism of the Breakup of Liquid Jets," *AIAA Journal*, Vol. 28, No. 1, 1990, pp. 120-126.
[5]Lin, S. P. and Ibrahim, E. A., "Instability of a Viscous Liquid Jet Surrounded by a Viscous Gas in a Vertical Pipe," *Journal of Fluid Mechanics*, Vol. 218, Sept. 1990, pp. 641-658.
[6]Squire, H. B, "Investigation of the Instability of a Moving Fluid Film," *British Journal of Applied Physics*, Vol. 4, June 1953, pp. 167-169.
[7]Taylor, G. I., "The Dynamics of Thin Sheets of Fluid," *Proceedings of the Royal Society of London*, Vol. A253, Dec. 1959, pp. 289-321.
[8]Hagerty, W. W., and Shea, J. F., "A Study of the Instability of Plane Fluid Sheets," *Journal of Applied Mechanics*, Vol. 22, ec. 1955, pp. 509-514.
[9]Dombrowski, N., and Johns, W. R., "The Aerodynamic Instability and Disintegration of Viscous Liquid Sheets," *Chemical Engineering Science*, Vol. 18, No. 3, 1963, pp. 203-214.
[10]Li, X., and Tankin, R. S., "On the Instability of a Two-Dimensional Viscous Liquid Sheets," *Journal of Fluid Mechanics*, Vol. 226, May 1991, pp. 425-443.
[11]Clark, C. J., and Dombrowski, N., "Aerodynamic Instability and Disintegration of Inviscid Liquid Sheets," *Proceedings of the Royal Society of London*, Vol. A329, No. 1579, 1972, pp. 467-478.
[12]Crapper, G. D., Dombrowski, N., and Pyott, G. A. D., "Large Amplitude Kelvin-Helmholtz Waves on Thin Liquid Sheets," *Proceedings of the Royal Society of London*, Vol. A342, No. 1629, 1975, pp. 209-224.
[13]Rangel, R. H., and Sirignano, W. A., "Nonlinear Growth of Kelvin-Helmholtz Instability: Effect of Surface Tension and Density Ratio," *Physics of Fluids*, Vol. 31, No. 7, 1988, pp. 1845-1855.
[14]Rangel, R. H., and Sirignano, W. A., "The Linear and Nonlinear Shear Instability of a Fluid Sheet," *Physics of Fluids A*, Vol. 3, No. 10, 1991, pp. 2392-2400.
[15]Rangel, R. H., and Hess, C., "Nonlinear Spatial Instability of a Fluid Sheet," *AIAA Paper 90-0118*, Jan. 1990.
[16]Lin, S. P., Lian, Z. W., Creighton, B. J., "Absolute and Convective Instability of a Liquid Sheet," *Journal of Fluid Mechanics*, Vol. 220, Nov. 1990, pp. 673-689.
[17]Crapper, G. D., Dombrowski, N., Jepson, W. P., and Pyott, G., "A Note on the Growth of Kelvin-Helmholtz Waves on Thin Liquid Sheets," *Journal of Fluid Mechanics*, Vol. 57, Pt. 4, 1973, pp. 671-672.
[18]Keller, J. B., Rubinow, S. I., and Tu, Y. O., "Spatial Instability of a Jet," *Physics of Fluids*, Vol. 16, Dec. 1972, pp. 2052-2055.

[19]Lin, S. P., and Kang, D. J., "Atomization of a Liquid Jet," *Physics of Fluids*, Vol. 30, No. 7, 1987, pp. 2000-2006.
[20]Huerre, P., and Monkewitz, P. A., "Local and Global Instabilities in Spatially Developing Flows," *Annual Review of Fluid Mechanics*, Vol. 22, 1990, pp. 473-537.
[21]Chuech, S. G., "A Comparative Study of Temporal and Spatial Instabilities of a Two-Dimensional Liquid Sheet," *Proceedings of the Winter Annual Meeting of the American Society of Mechanical Engineers*, HTD-Vol. 187, Dec. 1991, pp. 19-25.
[22]Tomotika, S. "On the Instability of a Cylindrical Thread of a Viscous Liquid Surrounded by Another Viscous Fluid," *Proceedings of the Royal Society*, Vol. 150, Series A, No. 870, 1935, pp. 322-337.
[23]Levich, V. G., *Physicochemical Hydrodynamics*, Prentice Hall, Englewood Cliffs, NJ 1962, p. 600.
[24]Muller, D. E., "A Method for Solving Algebraic Equations Using an Automatic Computer," *Mathematical Tables and Aids to Computation*, Vol. 10, No. 5, 1956, pp. 208-215.
[25]Gaster, M., "A Note on the Relation Between Temporally-Increasing and Spatially-Increasing Disturbances in Hydrodynamic Stability," *Journal of Fluid Mechanics*, Vol. 14, Pt. 2, Oct. 1962, pp. 222-224.
[26]Dombrowski, N., and Fraser, R. P., "A Photographic Investigation into the Disintegration of Liquid Sheets," *Philosophical Transactions of the Royal Society of London*, Vol. A247, Sept. 1954, pp. 101-130.
[27]Dombrowski, N., and Hooper, P. C., "The Effect of Ambient Density on Drop Formation in Sprays," Chemical Engineering Science, Vol. 17, April 1962, pp. 291-305.
[28]Dombrowski, N., Hasson, D., and Ward, D. E., "Some Aspects of Liquid Flow Through Fan Spray Nozzles," *Chemical Engineering Science*, Vol. 12, 1960, pp. 35-50.
[29]Taylor, G. I., "Formation of Thin Flat Sheets of Water," *Proceedings of the Royal Society of London A*, Vol. 259, November 1960, pp. 1-17.
[30]Weihs, D., and Frankel, I., "Equilibrium Shape and Stability of a Liquid Cylinder in Cross Flow at Low Weber Number," *Journal of Fluid Mechanics*, Vol. 116, 1982, pp. 393-409.
[31]Weber, C., *Z. Angew. Math. Mech.*, Vol. 11, 1931, pp. 136.
[32]Hasson, D. and Mizrahi, J., *Transactions of the Institute of Chemical Engineers*, Vol. 39, 1961, pp. 415.
[33]Mansour, Adel and Chigier, N., "Disintegration of Liquid Sheets," *Physics of Fluids A*, Vol. 2, No. 5, May 1990, pp. 706-719.
[34]Ibrahim, E. A., "Spatial Instability of a Viscous Liquid Sheet," *Journal of Propulsion and Power*, Vol. 11, No. 1, 1995, pp. 146-152.